Translational thresholds in a core circadian clock model

Paula S. Nieto* and C. A. Condat

Instituto de Física Enrique Gaviola (IFEG)-CONICET and Facultad de Matemática, Astronomía, Física y Computación, Universidad Nacional de Córdoba, Ciudad Universitaria, CP:X5000HUA Córdoba, Argentina

(Received 15 January 2019; revised manuscript received 11 June 2019; published 15 August 2019)

Organisms have evolved in a daily cyclic environment, developing circadian cell-autonomous clocks that temporally organize a wide range of biological processes. Translation is a highly regulated process mainly associated with the activity of microRNAs (miRNAs) at the translation initiation step that impacts on the molecular circadian clock dynamics. Recently, a molecular titration mechanism was proposed to explain the interactions between some miRNAs and their target mRNAs; new evidence also indicates that regulation by miRNA is a nonlinear process such that there is a threshold level of target mRNA below which protein production is drastically repressed. These observations led us to use a theoretical model of the circadian molecular clock to study the effect of miRNA-mediated translational thresholds on the molecular clock dynamics. We model the translational threshold by introducing a phenomenological Hill equation for the kinetics of PER translation and show how the parameters associated with translation kinetics affect the period, amplitude, and time delays between clock mRNA and clock protein expression. We show that our results are useful for analyzing experiments related to the translational regulation of negative elements of transcriptional-translational feedback loops. We also provide new elements for thinking about the translational threshold as a mechanism that favors the emergence of circadian rhythmicity, the tuning of the period-delay relationship and the cell capacity to control the protein oscillation amplitude with almost negligible changes in the mRNA amplitudes.

DOI: 10.1103/PhysRevE.100.022409

I. INTRODUCTION

From bacteria to humans, organisms have evolved in a daily cyclic environment and, as a consequence, developed circadian (*circa* = near; *dian* = a day) cell-autonomous time-keeping mechanisms (clocks) [1]. These clocks temporally organize a wide range of biological processes in living beings, optimizing their physiology and metabolism to improve fitness and survival. For instance, the forcing of the cell cycle by the circadian oscillator seems to increase cell variability in clonal cell populations [2]. A common design across species is observed in their molecular clockwork, involving a set of clock genes and proteins that interact in transcriptional-translational feedback loops (TTFL) [3,4]. In animals, positive elements of the core loop (BMAL1 and CLOCK in mammals; CYCLE and CLOCK in flies) activate the transcription of target genes, including the negative elements of the loop (*Per 1, 2, 3* and *Cry 1, 2* in mammals; *Per* and *Tim* in flies). Once negative elements are translated, they are the target of post-translational modifications and can heterodimerize, translocate into the nucleus, and repress the transcriptional activity of positive elements by directly binding to them. Thus, negative elements repress their own transcription. Turnover of negative elements results in the eventual derepression of the positive elements and the reactivation of clock gene expression, starting the core loop again after approximately 24 h. Secondary loops, both in mammals and flies, confer robustness and precision to the molecular clock, and a high robustness in the period implies higher plasticity in the phase, which is important to adapt to sudden environmental changes [5]. In addition, the molecular circadian clock is able to regulate the expression of downstream genes (clock controlled genes, *ccg*) and thus control cell physiology and metabolism [6].

Although transcriptional regulation has been considered the main mechanism involved in the maintenance of the steady-state levels of mRNAs associated with clock genes, recent evidence has shown that transcriptional modulation is only one of many layers (i.e., splicing, termination, polyadenylation, nuclear export, microRNA regulation, translation, and RNA decay) of circadian regulation in gene expression [7–9]. Specifically, translational regulation impacts on the circadian clock and its outputs, contributing to the fine-tuning of circadian rhythms dynamics [10].

Translational activation through regulators acting over clock transcripts has been described for flies and mammals [11–14]; and the dynamical changes of the clockwork derived from their activity have been previously considered in the context of a basic core clock theoretical model [15]. On the other hand, translational repression is a much less understood process, mainly associated with the microRNA (miRNA) activity at the initiation step of translation, which is also the rate-limiting step [16].

miRNAs are noncoding RNAs approximately 22 nucleotides long that, through binding to specific sequences within target mRNAs, mediate two main modes of gene expression silencing: (i) mRNA decay and (ii) *pure* translational repression. Regarding the first, a detailed picture of the mechanisms underlying the miRNA-mediated mRNA decay

*Corresponding author: pnieto1@famaf.unc.edu.ar

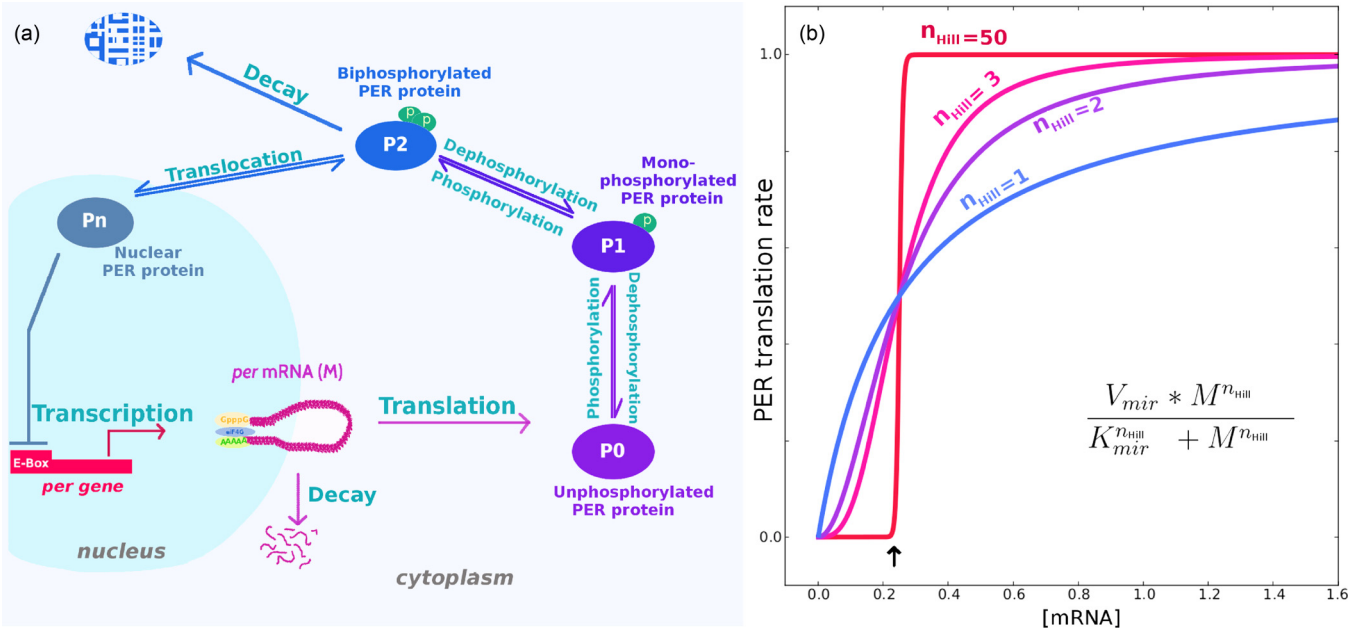

FIG. 1. (a) Our deterministic model. The model is based on Refs. [15,26] and contains five variables: *per* mRNA (M), unphosphorylated PER protein (P_0), monophosphorylated PER protein (P_1), biphosphorylated PER protein (P_2), and the nuclear PER protein (P_n). The scheme also highlights the biochemical processes whose kinetics we model. (b) Scheme of the translation kinetics. We considered that the effective kinetics of translation follows a sigmoidal relationship with the *per* mRNA concentration. The Hill exponent (n_{Hill}) effectively introduces a threshold in the kinetics. The emergence of this threshold effect leads to two regimes: (i) at low mRNA concentrations the process exhibits a slowdown of the kinetics as n_{Hill} increases; (ii) after reaching a given (threshold) mRNA concentration, the kinetics of the process changes and accelerates with n_{Hill} until the saturation becomes evident. The threshold mRNA concentration is clearly observed in the extreme case $n_{\text{Hill}} = 50$ (arrow).

has emerged from multiple experimental analyses [10,16,17] and theoretical studies [18,19]. By contrast, *pure* miRNA-mediated translational repression (i.e., without mRNA decay) has been observed in flies, zebrafish, and humans [20], but the precise mechanisms involved require further understanding [10].

Recently, a molecular titration mechanism was proposed to explain the interactions between some miRNAs and their target mRNAs [21,22]. Evidence supporting this mechanism suggests that regulation by miRNA is a nonlinear process that yields a threshold level of target mRNA below which protein production is drastically repressed, while above this mRNA threshold protein production is active and sensitive to the mRNA transcription [23,24]. Taking into account these observations, we sought to study the effect of applying a translational threshold on the molecular clock dynamics. To accomplish this, we use a theoretical model of the circadian molecular clock previously proposed to study other aspects of the circadian molecular behavior [15,25,26]. By phenomenologically describing the effective kinetics of PER synthesis in terms of a Hill equation, we show that it is posible to capture the main feature of a miRNA-mRNA titration-based mechanism: the threshold-like behavior. In addition, we show how the parameters associated with the Hill equation affect the period, amplitude, and the time lags between clock mRNA and clock protein expression (delays). Our results are useful for analyzing previous experimental observations related to translational regulation of negative elements of transcriptional-translational feedback loops. We provide new elements for thinking about the translational regulation as a mechanism that favors the emergence of circadian rhythmicity, the tuning of the period-delay relationship and the cell capacity to control the protein oscillation amplitude with almost negligible changes in the mRNA amplitudes.

II. METHODS

A. Mathematical model

TTFL dynamics can be qualitatively described by a conceptual model [Fig. 1(a)] that can be transformed into a mathematical model by the selection of adequate equations and parameters representing the biochemical processes involved in the core molecular clock [27]. In a pioneering work, Goldbeter showed how a Goodwin oscillator can be adapted to describe the circadian cell biology, keeping the model as simple as possible [25]. We based our study on a Goldbeter structure-grounded model proposed by Gonze and co-workers [26]. Gonze's deterministic version has exactly the same functional form (terms and equations) as the original model [25]. The differences are related to the parameter values, which we took from a more recent paper [26] and we already used in a previous work from our laboratory [15].

Briefly, the model takes into account core clock processes involved in the negative feedback exerted by a protein (PER) on its own expression by considering five variables: The *Per* mRNA (M), the unphosphorylated PER protein (P_o), the monophosphorylated protein (P_1), the biphosphorylated protein (P_2), and the the nuclear protein (P_n). The total protein (P_t) is calculated as the sum of all PER species ($P_t = P_0 + P_1 + P_2 + P_n$).

Similarly to our previous work [15], here we assume that the core processes involved in circadian rhythmicity occur with same kinetics as in Ref. [26], except for PER translation, which is assumed to follow a Hill-type dependence on the mRNA concentration [Fig. 1(b)]. Thus, the differential equations of our model are as follows:

$$\frac{dM}{dt} = v_s \frac{K_i^{nt}}{K_i^{nt} + P_n^{nt}} - v_m \frac{M}{K_m + M}, \tag{1}$$

$$\frac{dP_0}{dt} = V_{\text{mir}} \frac{M^{n\text{Hill}}}{K_{\text{mir}}^{n\text{Hill}} + M^{n\text{Hill}}} - V_1 \frac{P_0}{K_1 + P_0} + V_2 \frac{P_1}{K_2 + P_1}, \tag{2}$$

$$\frac{dP_1}{dt} = V_1 \frac{P_0}{K_1 + P_0} - V_2 \frac{P_1}{K_2 + P_1} - V_3 \frac{P_1}{K_3 + P_1} + V_4 \frac{P_2}{K_4 + P_2}, \tag{3}$$

$$\frac{dP_2}{dt} = V_3 \frac{P_1}{K_3 + P_1} - V_4 \frac{P_2}{K_4 + P_2} - k_1 P_2 + k_2 P_n - v_d \frac{P_2}{K_d + P_2}, \tag{4}$$

$$\frac{dP_n}{dt} = k_1 P_2 - k_2 P_n. \tag{5}$$

A detailed description of parameter meaning and values, as well as model assumptions, can be found in the Appendix.

It is worth noting that this mathematical model has a level of complexity intermediate between other either more simplistic or more detailed models. The first have a low number of variables and parameters, which makes them analytically tractable but difficult to associate to real quantities. The second may have a more direct biological interpretation but their high number of variables and parameters reduces their predictive capacity. As discussed previously, very detailed mathematical models do not guarantee good consistency between their predictions and experimental data, but the Goodwin-based models, like the one proposed here, are closer to capturing qualitatively the oscillatory system features [28].

1. Translational kinetics

The way in which some miRNAs interact with their targets can be described in terms of a titration mechanism, characterized by a *threshold* in the translation [23,24]. Here we model this effect by considering a Hill equation [Fig. 1(b)] for the PER translational kinetics. This phenomenological modeling approach captures the main feature of the titration-based mechanism, i.e., the threshold effect [29], while it keeps the model simpler by not explicitly considering the miRNAs concentration as an additional variable. The Hill equation,

$$v_{\text{translation}} = \frac{V_{\text{mir}} M^{n_{\text{Hill}}}}{K_{\text{mir}}^{n_{\text{Hill}}} + M^{n_{\text{Hill}}}}, \tag{6}$$

is characterized by three parameters (that we call *translational parameters*):

(i) n_{Hill} is the parameter that controls the sharpness of the translational threshold: The bigger the n_{Hill} value, the sharper the translational repression at low mRNA levels [Fig. 1(b)]. This parameter does not have a *direct* molecular interpretation (i.e., as the miRNA concentration or the cooperativity of the miRNA binding sites at the mRNA). Instead, it is a parameter that indicates a general miRNA-based threshold effect.

(ii) V_{mir} is the parameter that controls the maximum PER translation rate. We biologically interpret this parameter as being proportional to the concentration of translational enhancers involved in the PER synthesis. For instance, in our previous work [15] we interpreted this parameter as related to the concentration of the TYF protein in the cell.

(iii) K_{mir} is the mRNA concentration at which the PER synthesis is one half of V_{mir}.

In this work we mainly focus on understanding how the translational parameters affect the dynamical properties of a core clock model. For other biochemical processes involved in the core clock we use the functions and parameter values reported in Refs. [15,25,26] (see Appendix).

B. Numerical integration

The system of five coupled differential equations was integrated using a fourth-order Runge-Kutta algorithm with 1×10^7 steps and a time step of 0.1 h. Before analyzing the stationary behavior of the system we discard the first 999,800 h of computation in order to eliminate transient effects. The results we present are the averages of 10 realizations, each one with random initial conditions. We have numerically explored the K_{mir}-V_{mir} planes for each value of n_{Hill} over, at least, nine orders of magnitude.

C. Period, delay, and amplitude estimation

For each value of K_{mir}-V_{mir} and n_{Hill} explored, an average period length was calculated from consecutive peaks and troughs within the M, P_0, and P_t time series. Then, an average over realizations was obtained and coded as pseudocolor in the K_{mir}-V_{mir} diagrams shown in Fig. 2. The standard deviation (SD) of the period in the colored regions was SD $< 1 \times 10^{-4}$ h for $n_{\text{Hill}} = 1$, SD < 0.012 h for $n_{\text{Hill}} = 2$, SD < 0.045 h for $n_{\text{Hill}} = 3$, SD < 0.015 h for $n_{\text{Hill}} = 4$, and SD < 0.2 h for $n_{\text{Hill}} = 50$. The same procedure was performed with the peak-to-trough amplitudes and the time lags between the M and P_0 peaks (or the M and P_t peaks).

D. Area quantification

In order to estimate the total and circadian areas explored in our simulations, we associate to each pair $K_{\text{mir}}(i)$-$V_{\text{mir}}(j)$ a rectangular element of surface with sides:

$$K_{\text{mir}}l = \frac{K_{\text{mir}}(i) - K_{\text{mir}}(i-1)}{2} + \frac{K_{\text{mir}}(i+1) - K_{\text{mir}}(i)}{2}, \tag{7}$$

$$V_{\text{mir}}l = \frac{V_{\text{mir}}(j) - V_{\text{mir}}(j-1)}{2} + \frac{V_{\text{mir}}(j+1) - V_{\text{mir}}(j)}{2}, \tag{8}$$

where i and j are the indices used to represent specific K_{mir} and V_{mir} values, respectively. This definition allows us to associate a rectangular area $A_{ij} = K_{\text{mir}}l \times V_{\text{mir}}l$ to each pair $K_{\text{mir}}(i)$-$V_{\text{mir}}(j)$. Depending on the system solution associated with a given $K_{\text{mir}}(i)$-$V_{\text{mir}}(j)$ pair, it is possible to group the corresponding areas A_{ij} in one of the following categories:

(1) The associated A_{ij} surface is included in the quantification of the total self-sustained oscillatory area when pairs $K_{\text{mir}}(i)$, $V_{\text{mir}}(j)$ yield a system with a periodic solution;

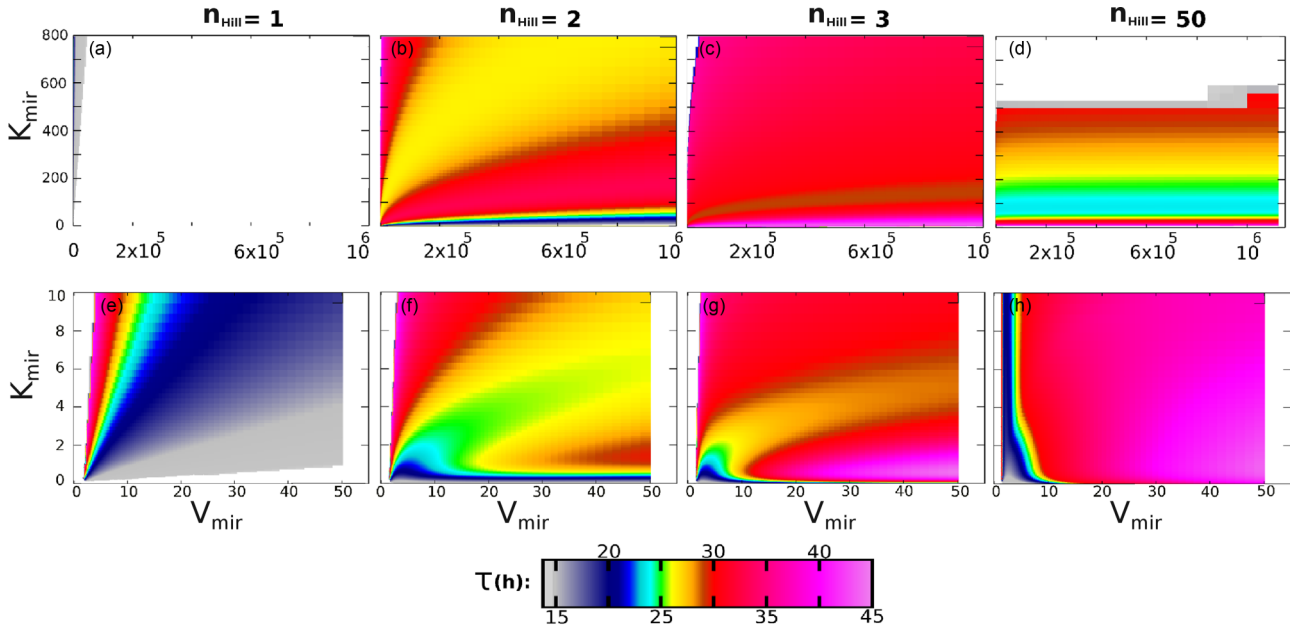

FIG. 2. The oscillation period (τ) depends on the translational parameters V_{mir}, K_{mir}, and n_{Hill}. Phase diagrams in the K_{mir}-V_{mir} subspace for $n_{\mathrm{Hill}} = 1$ [(a) and (e)], $n_{\mathrm{Hill}} = 2$ [(b) and (f)], $n_{\mathrm{Hill}} = 3$ [(c) and (g)], and $n_{\mathrm{Hill}} = 50$ [(d) and (h)] are shown. Top panels show the full explored range of the K_{mir} and V_{mir} parameters. Bottom panels show magnifications of the corresponding top panels within the [0–10] K_{mir} range and [0–50] V_{mir} range. White regions indicate pairs (K_{mir}-V_{mir}) that do not correspond to an oscillatory solution for the system. For those pairs (K_{mir}-V_{mir}) for which a periodic solution is obtained, a pseudocolor was assigned indicating the period (τ), as shown in the key.

(2) The A_{ij} surface is included in the quantification of the total circadian area when pairs $K_{\mathrm{mir}}(i)$-$V_{\mathrm{mir}}(j)$ yield a system with periodic solutions within the circadian range.

Both the total self-sustained oscillatory area and the the total circadian area are normalized by the total explored area, which is the sum of the A_{ij} for all the $K_{\mathrm{mir}}(i)$-$V_{\mathrm{mir}}(j)$ numerically explored. This procedure is followed for each realization at each explored n_{Hill} value. The corresponding standard deviation was also obtained and plotted for each n_{Hill}.

III. RESULTS

A. Oscillatory properties of the system and intrinsic period (τ)

We numerically explored the translational parameter space defined by K_{mir}, V_{mir}, and n_{Hill} (Fig. 2). For all the n_{Hill} values studied we found two regions, one where the system oscillates self-sustainedly (shown in pseudocolor) and the other where the system presents damped oscillations, which eventually evolve toward fixed points (white regions). Figure 3 reveals details of these spaces at small K_{mir}-V_{mir} values. For $n_{\mathrm{Hill}} = 1$ there is no translational threshold because the Hill equation reduces to a simple Michaelis-Menten equation. Results for this particular case were already reported [15].

Figure 2 qualitatively indicates that the oscillatory (colored) region within the translational parameter space (defined by K_{mir}, V_{mir}, and n_{Hill}) increases when $n_{\mathrm{Hill}} > 1$. This is quantitatively shown in Fig. 4 (black circles) which indicates that a moderate increase in n_{Hill} ($n_{\mathrm{Hill}} = 2$–4) leads to a maximum oscillatory region size within the translational K_{mir}-V_{mir} parameter plane. Further increases in the n_{Hill} parameter lead first to a decrease ($n_{\mathrm{Hill}} = 8$–12) and then to a new increase ($n_{\mathrm{Hill}} = 50$) in the size of the oscillatory region. This result strongly suggests that the inclusion of a moderate threshold effect in the PER translation (achieved by a modest n_{Hill} increase) promotes the emergence of self-sustained oscillations.

Circadian oscillations are defined as those with a period near 24 h. Nevertheless, the circadian period range experimentally measured in cells depends on animal species, cell type, coupling strength between cells, and output measured, among other factors [30–33]. Thus, for our purpose we define circadian periods as those whose length ranges from 20 to 28 h. Under this assumption, Fig. 4 (red circles) shows that the region where oscillations have circadian periods exhibits a maximal size when $n_{\mathrm{Hill}} = 2$. In addition, the probability of obtaining oscillations with long periodicities (infradian rhythms) increases as the translation threshold sharpens.

In summary, our results suggest that both the emergence of self-sustained oscillations and the circadian periodicity are favored by a moderate increase of n_{Hill} (i.e., a mild threshold). This seems to be a general finding since we observed a qualitatively similar behavior in a simpler, but similar, TTFL model (see the LGG1999 model section in the Appendix). Taking into account these results, our further analysis will mainly focus on the elucidation of the differences between the cases $n_{\mathrm{Hill}} = 1$ and $n_{\mathrm{Hill}} = 2$.

B. Time lag between per mRNA and total PER protein

Does a moderate threshold in PER translation significantly affect the time lags (delays) between clock mRNAs and proteins? In order to address this question, we measured the delays between the acrophases of *per* mRNA and total PER protein expression, both for $n_{\mathrm{Hill}} = 1$ and $n_{\mathrm{Hill}} = 2$. Figure 5(a) shows the results for $n_{\mathrm{Hill}} = 1$, which are consistent with those already reported in Ref. [15]: At constant K_{mir} (i.e.,

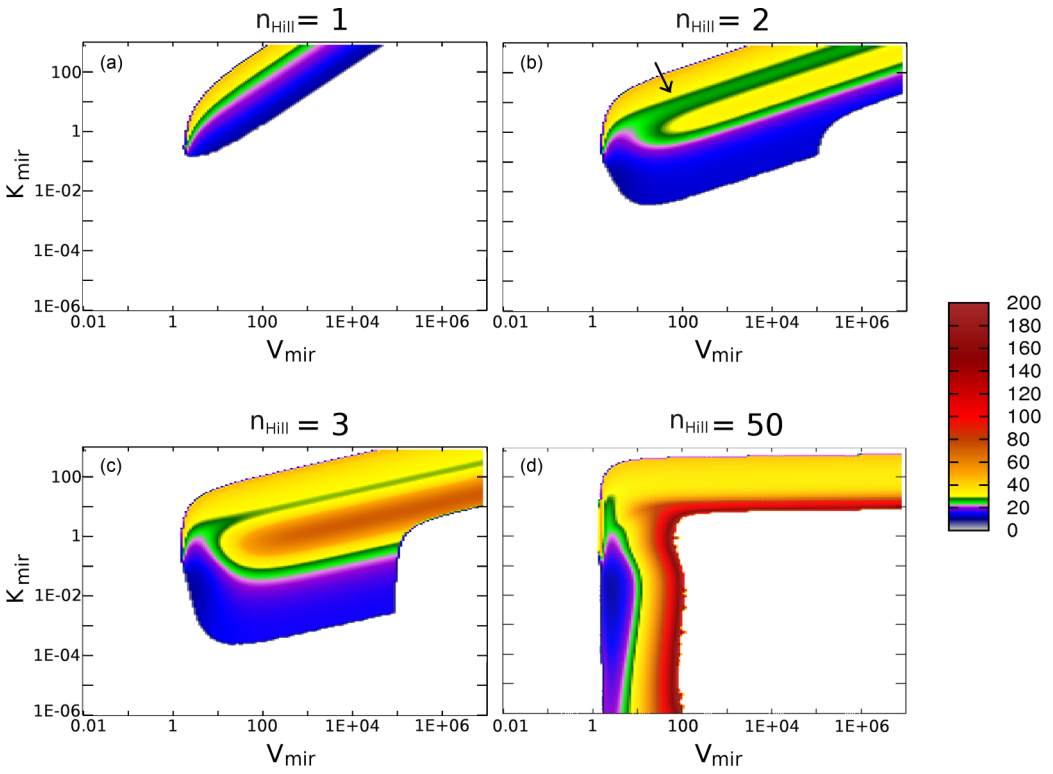

FIG. 3. Phase diagrams in the V_{mir}-K_{mir} subspace for $n_{Hill} = 1$ (a), $n_{Hill} = 2$ (b), $n_{Hill} = 3$ (c), and $n_{Hill} = 50$ (d). Pseudocolor indicates the K_{mir}-V_{mir} pairs for which a periodic solution is obtained. The τ length is shown in the key. White regions indicate K_{mir}-V_{mir} pairs that do not correspond to an oscillatory solution for the system. These diagrams are exactly the same as those shown in Fig. 2 but in a logarithmic scale, which allows us to observe details at small K_{mir} - V_{mir} values. The arrow in (b) was included as a comparison tool: It indicates the yellow region of Fig. 2(b).

a K_{mir} isoline, plotted in a specific color), there is a monotonic increase of the delays with the period length, a behavior that is characteristic for most of the K_{mir}-V_{mir} pairs explored. An exception to this behavior is shown in Fig. 6 [a magnification of Fig. 5(a)], where we observe that in a region of high K_{mir} and V_{mir} the delay is a decreasing function of the period (note that in this region periods are well into the ultradian regime).

When $n_{Hill} = 2$ [Fig. 5(b), see also Fig. 7] the delays become nonmonotonic multivalued functions of the period length. This means that for a single K_{mir} isoline there are several delay values (defined by V_{mir}) that can generate the same period length. The global comparison of both conditions [$n_{Hill} = 1$ vs. $n_{Hill} = 2$, Fig. 5(c)] allows us to highlight that $n_{Hill} = 2$ increases the number of K_{mir} isolines from which it is possible to obtain an oscillatory system. This is consistent with the results shown in Fig. 4. In addition, Fig. 5(c) reveals that for $n_{Hill} = 2$ the K_{mir} isolines *twist* when the delay values are small (roughly, below 5 h) or, in other words, when V_{mir} is high.

Indeed, if we take into account that the delay ranges previously reported were between 6 and 8 h, [34,35], and confine our analysis to periods within the previously defined circadian range (20–28 h), we observe a monotonic increase of the delay with the period length for $n_{Hill} = 2$ [Figs. 5(d)–5(f)], just as it occurs for $n_{Hill} = 1$. Nevertheless, two qualitative differences were observed between the cases $n_{Hill} = 1$ and $n_{Hill} = 2$. First, while a big number of K_{mir} isolines are observed for $n_{Hill} = 1$ [Fig. 5(d)], only a subset of them are observed for $n_{Hill} = 2$ [Fig. 5(e)]. This means that the dynamic range of K_{mir}-V_{mir} pairs enabling the experimentally observed circadian behavior is reduced even if the oscillation diversity is favored by $n_{Hill} = 2$. Second, the monotonic relationship between delays and periods exhibits a steeper slope for $n_{Hill} = 2$ than for $n_{Hill} = 1$ [Fig. 5(f)]. This has two consequences: On one hand, changes in delays are associated with smaller changes in the period length when $n_{Hill} = 2$ than when $n_{Hill} = 1$. We can interpret this as meaning that $n_{Hill} = 2$ confers an increase in period robustness in the presence of putative delay perturbations generated by fluctuations in V_{mir}. On the other hand, $n_{Hill} = 2$ yields a subset of K_{mir} isolines [see the black lines in the upper left corner of Fig. 5(f)] for which circadian oscillations exhibit longer delays than those corresponding to any of the K_{mir} isolines obtained with $n_{Hill} = 1$. This means that $n_{Hill} = 2$ opens the possibility of tuning the K_{mir}-V_{mir} values to obtain circadian oscillations within the range of 20–26 h with long delays (6–8 h).

The preceding global analysis does not allow us to examine whether the increase in n_{Hill} introduces time delays by itself (that is, when the same K_{mir}-V_{mir} pair is considered). In order to shed light on this question, we compare individual K_{mir} isolines for $n_{Hill} = 1$ and $n_{Hill} = 2$ (Fig. 8). Since the results strongly depend on V_{mir} we analyze separately two regions of the K_{mir}-V_{mir} plane, one within the range of experimentally

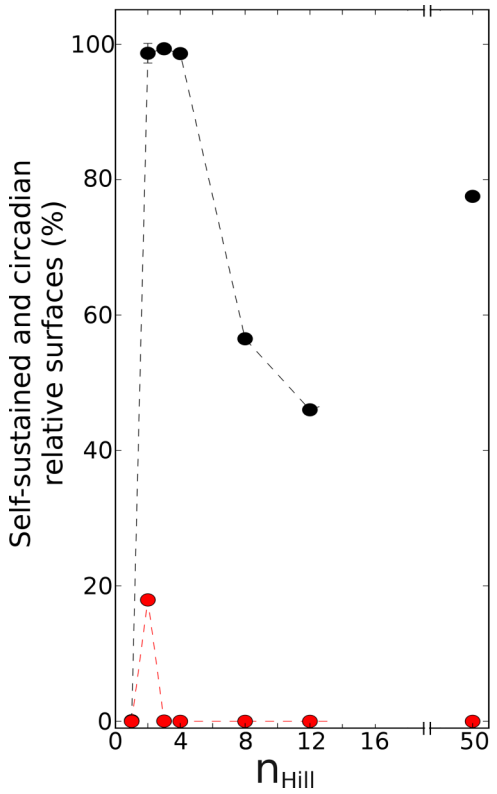

FIG. 4. For each n_{Hill} (1, 2, 3, 4, 8, 12, and 50) examined, it is possible to define the total surface associated with the pairs (K_{mir}-V_{mir}) covered in our study. Once this is known, the relative areas of the surfaces where self-sustained (black circles, upper line) or circadian (red circles, bottom line) oscillations emerge can be estimated. We observe that the probability of finding a pair (K_{mir}-V_{mir}) that gives rise to a periodic solution is bigger when $n_{\mathrm{Hill}} > 1$ and that the emergence of circadian oscillations is highly favored when $n_{\mathrm{Hill}} = 2$.

observed delays and periodicities (i.e., within the violet rectangle of Fig. 8) and the other outside of the experimentally observed periods and delays (i.e., outside the violet rectangle of Fig. 8). Within the range of experimentally observed behaviors, an increase of n_{Hill} typically leads to a shortening of both delay and period (red to black triangles in Figs. 8(b)–8(f)]. On the other hand, outside of the experimentally observed ranges, delay-period pairs present a diversity of behaviors when going from $n_{\mathrm{Hill}} = 1$ to $n_{\mathrm{Hill}} = 2$: delay lengthening with period shortening; delay and period lengthening [red to black squares in Figs. 8(a)–8(f)]; delay and period shortening; period lengthening with delay shortening, among other possibilities.

Summarizing, the inclusion of a moderate threshold effect in the PER translation generates oscillations within the observed range of periods and delays. Within this range, the longer the delay, the longer the period, which is similar to what is observed for $n_{\mathrm{Hill}} = 1$. In addition, $n_{\mathrm{Hill}} = 2$ opens the possibility of obtaining a K_{mir}-V_{mir} region that yields circadian oscillations with very long delays and increases the period robustness against delay perturbations. Last, within the range of observed delays and periods, an increase from $n_{\mathrm{Hill}} = 1$ to $n_{\mathrm{Hill}} = 2$ shortens both delays and periods.

C. Temporal evolution and oscillation amplitudes

In order to understand the effects of n_{Hill} on the mRNA (M) and unphosphorylated protein (P_0) dynamics, we investigate the correlations between the P_0 and M peak-to-trough amplitudes (Fig. 9) for the whole range of K_{mir}-V_{mir} pairs studied in Fig. 2. This global analysis sheds light on the evolution of the amplitude differences as n_{Hill} changes. As expected, we observe that there is a nonlinear relationship between the amplitudes of P_0 and M, even if $n_{\mathrm{Hill}} = 1$ [Fig. 9(a)]. Each black curve there represents the P_0-M relationship at constant K_{mir} (K_{mir} isoline). In cyan we highlight the P_0-M amplitude points corresponding to oscillations within the circadian range. As n_{Hill} increases from $n_{\mathrm{Hill}} = 1$ [Fig. 9(a)] to $n_{\mathrm{Hill}} = 2$ [Fig. 9(b)], the range of P_0 peak-to-trough amplitudes increases, but there is no significant change in the M amplitude range (compare the P_0 scales in Figs. 9(a) and 9(b)]. This result suggests that a threshold effect in PER translation leads to a strong growth of the P_0 amplitude with almost no changes in the M amplitude. For both $n_{\mathrm{Hill}} = 1$ and 2, most of the K_{mir} isolines are concave functions, displaying a V_{mir} value that maximizes the P_0 amplitude for a given M amplitude. Exceptions to this behavior are observed for very high values of K_{mir} (see Fig. 10). In addition, when $n_{\mathrm{Hill}} = 2$, but not when $n_{\mathrm{Hill}} = 1$, a subset of K_{mir} isolines exhibits a peak (maximal P_0 amplitude) that corresponds to oscillations within the circadian range [cyan dots in Fig. 9(b)]. Similar results were found when we analyzed the geometrical amplitude, which gives an estimation of the mean concentration of M and P_0 (results not shown).

Figure 11 shows two examples of the temporal evolution of the variables per mRNA (M), unphosphorylated PER protein (P_0), and total PER protein (P_t) for $n_{\mathrm{Hill}} = 1$ (red lines) and $n_{\mathrm{Hill}} = 2$ (black lines). Figures 11(a)–11(c) correspond to the pair K_{mir}-$V_{\mathrm{mir}} = 0.3548$–$2.2387$, represented with triangles inside of the violet rectangle shown in Fig. 8(b). This exemplifies the general conclusion obtained from the global analysis of Fig. 9: An increase of n_{Hill} leads to an increase of the P_0 and P_t peak-to-trough amplitudes without a significative increase of the mRNA peak-to-trough amplitude. Besides, this figure suggests that the period and delay shortenings when n_{Hill} increases from 1 to 2 are consequences of the advanced P_0 and P_t accumulation phases for $n_{\mathrm{Hill}} = 2$ as compared with $n_{\mathrm{Hill}} = 1$, which is revealed by the steeper slope observed for $n_{\mathrm{Hill}} = 2$ in the upswing phase of the protein dynamics.

Figures 11(d)–11(f) correspond to the pair K_{mir}-$V_{\mathrm{mir}} =$ 0.3548-3.5481, represented with squares outside of the violet rectangle of Fig. 8(b). Unlike the M behavior shown in Fig. 11(a), Fig. 11(d) shows that the M amplitude increases with an increase of n_{Hill}. Moreover, this example indicates that there is a parameter set for which the model displays period and delay lengthenings when n_{Hill} increases from 1 to 2. Although the slope observed in the upswing phase of the protein dynamics is steeper for $n_{\mathrm{Hill}} = 2$ than for $n_{\mathrm{Hill}} =$ 1, the increase of n_{Hill} produces a flattening of the trough. This latter effect probably contributes to elongate both the period and the delay. Figure 12 shows similar results for the pairs K_{mir}-$V_{\mathrm{mir}} = 1.5849$-$3.5481$ [Figs. 12(a)–12(c)] and K_{mir}-$V_{\mathrm{mir}} = 1.5849$–$22.387$ [Figs. 12(c), 12(d), and 12(f)], corresponding to the triangles (inside of the violet rectangle)

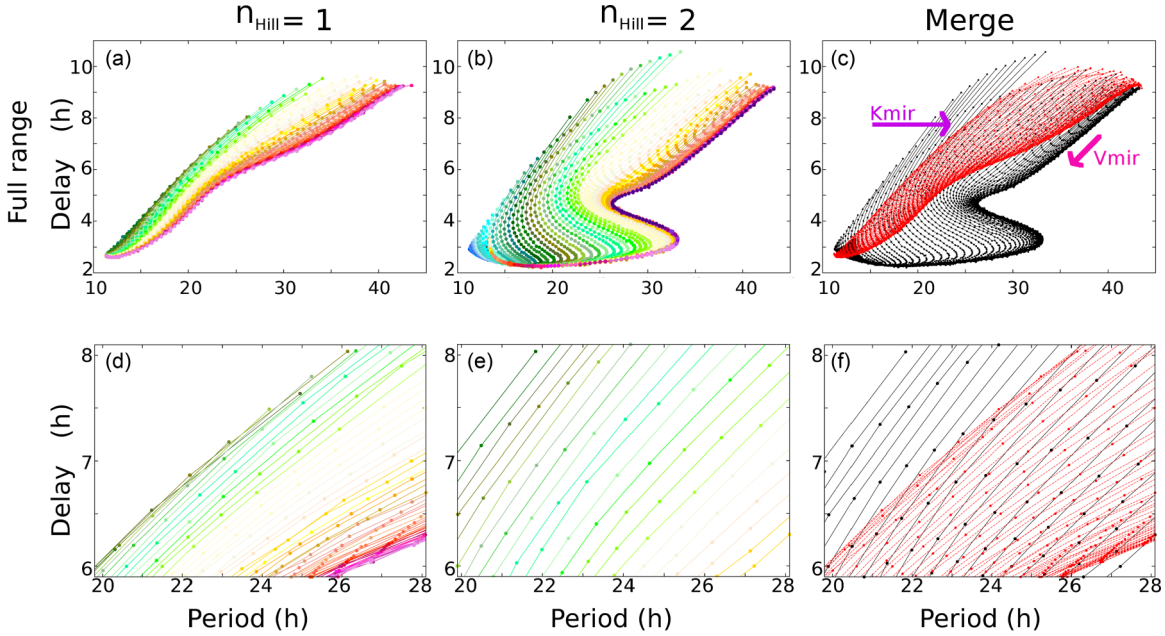

FIG. 5. The translational threshold affects the period-delay relationship. Time lags between *mRNA* and total PER protein (delays) contribute to define the periodicity (τ) of the oscillations. The correlation between delays and τ for each K_{mir}-V_{mir} pair explored allows us to observe how delays contribute to period length. Each colored curve represents a K_{mir} isoline, that is, the K_{mir}-V_{mir} pairs that share the same K_{mir} value. (a) For $n_{Hill} = 1$ the delay increases monotonically with τ. Gray K_{mir} isolines represent K_{mir} values from 0.16 to 0.45; blue K_{mir} isolines represent K_{mir} values from 0.5 to 3.2; green K_{mir} isolines represent K_{mir} values from 3.55 to 44.7; yellow-magenta K_{mir} isolines represent K_{mir} values from 50 to 177. (b) For $n_{Hill} = 2$, the period is a strongly nonlinear function of the delay. In Fig. 7 we show a detailed description of K_{mir} isolines subsets when $n_{Hill} = 2$. (c) A combination of K_{mir} isolines shown in (a) (displayed in red) and K_{mir} isolines shown in (b) (displayed in black) facilitates the comparison between $n_{Hill} = 1$ and $n_{Hill} = 2$. Pink arrow indicates the direction of V_{mir} increase whereas violet arrow indicates the direction of K_{mir} increase. Panels (d), (e), and (f) are magnifications of the circadian regions in (a), (b), and (c), respectively.

or the squares (outside of the violet rectangle) shown in Fig. 8(e), respectively.

D. Sensitivity analysis

Next, we discuss the sensitivity of the period to changes in various relevant model parameters. Thus, we proceed to determine how the period is altered when each parameter (other than V_{mir} and K_{mir}) is varied (one at a time) by, at least, ± 100 of their original value (see Table 1) and we compare the results for $n_{Hill} = 2$ to those for $n_{Hill} = 1$. Relevant results are shown in Fig. 13 while the cases shown in Fig. 14 did not exhibit significant changes between the two conditions tested here.

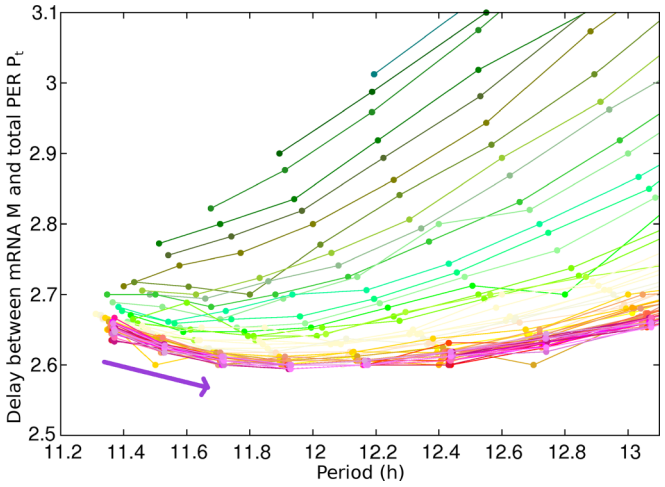

FIG. 6. Detail of Fig. 5(a). High K_{mir} isolines exhibit a minimum delay for ultradian cycles. The arrow indicates the direction of V_{mir} decrease. K_{mir} decreases from the bottom up.

Figure 13 shows the dependence of the period with the parameters related to mRNA dynamics. Figure 13(a) shows the period sensitivity with the Hill exponent for the repression of mRNA transcription (n_t). For both values of n_{Hill} the period decreases with nt, but the decrease has a smaller slope for $n_{Hill} = 2$. This means that the period sensitivity to nt decreases when a moderate threshold is included in the translation kinetics. In addition, for $n_{Hill} = 2$ the window for the occurrence of oscillations extends to lower values of n_t. This agrees with the results of Kurosawa *et al.*, which indicate that an increase in the nonlinearity augments the likelihood of oscillatory behavior [36]. Figure 13(b) shows the period sensitivity to the mRNA (M) transcription rate (v_s). For both values of n_{Hill}, the period length initially decreases, reaches a minimum (near $v_s = 0.4$), and then increases as v_s increases. For $v_s < 0.5$ the increase in n_{Hill} leads to a slight shortening of the period length, whereas for $v_s > 0.5$ an increase in n_{Hill} leads to period lengthening (with a higher slope for $n_{Hill} = 2$ than for $n_{Hill} = 1$). Thus, globally, the period sensitivity to v_s increases when n_{Hill} changes from 1 to 2. Figure 13(c) shows the period sensitivity to the Michaelis constant for mRNA degradation (K_m) and indicates that the approximately linear increase of the period with K_m has a higher slope (more sensitivity) for $n_{Hill} = 2$.

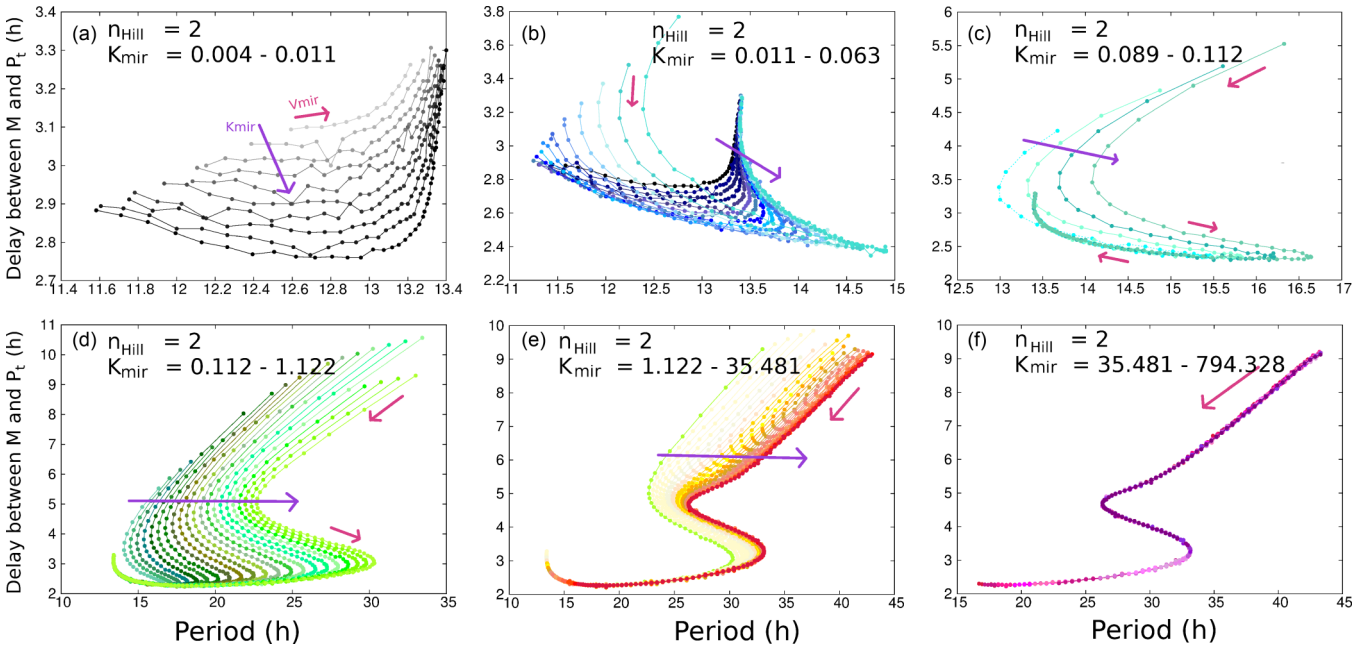

FIG. 7. Details of Fig. 5(b) (K_{mir} isolines for $n_{\mathrm{Hill}} = 2$). Evolution of K_{mir} isoline morphology. For very low values of K_{mir} (a), the isolines do not intersect and increasing V_{mir} always leads to a period increase. For intermediate values of K_{mir} [(b) to (e)], the isolines twist and there is a period domain for which we observe more than one possible value of the delay for each period length; increasing V_{mir} may lead to increases or decreases in period length. For high values of K_{mir} (f) the isolines collapse on a strongly nonlinear curve. Pink arrows indicate the direction of V_{mir} increase, whereas violet arrows indicate the direction of K_{mir} increase.

Figure 15 shows the dependence of the period with parameters related to protein degradation. Figure 15(a) shows the dependence of the period with the maximum rate of biphosphorylated protein degradation (v_d), whereas Fig. 15(b) shows the period dependence with the Michaelis constant of biphosphorylated protein (P_2) degradation, K_d. Increasing v_d leads to a monotonical increase in the period, which is smaller for $n_{\mathrm{Hill}} = 2$. This means that the period sensitivity to v_d decreases when n_{Hill} changes from 1 to 2. On the other hand, increasing the Michaelis constant K_d in the protein decay term leads to a monotonical period shortening, which is softer for $n_{\mathrm{Hill}} = 2$, and therefore the period sensitivity to K_d also

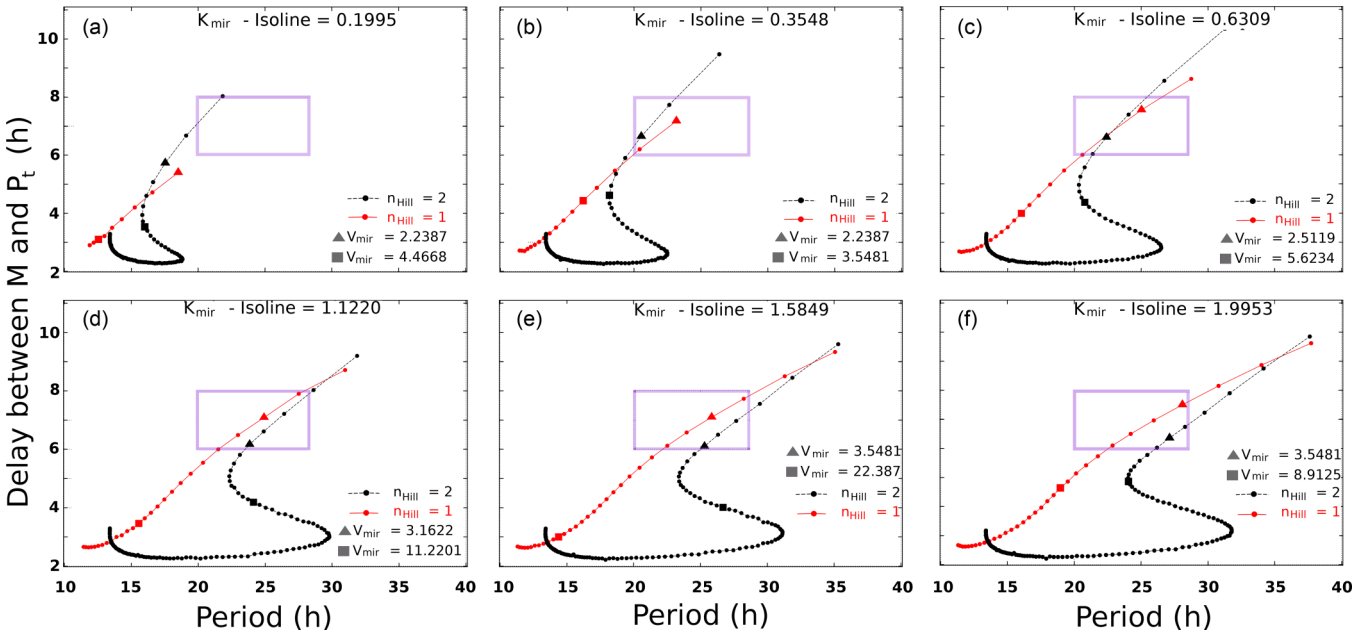

FIG. 8. Individual K_{mir} isolines for $n_{\mathrm{Hill}} = 1$ (monotonically crescent curves) and $n_{\mathrm{Hill}} = 2$ (S-like curves). The rectangles enclose the experimentally observed values of the period and delay. For all the values of K_{mir} considered, both the period and the delay shorten with increasing V_{mir} inside of these rectangles. A more complicated picture is observed outside the rectangles (see text).

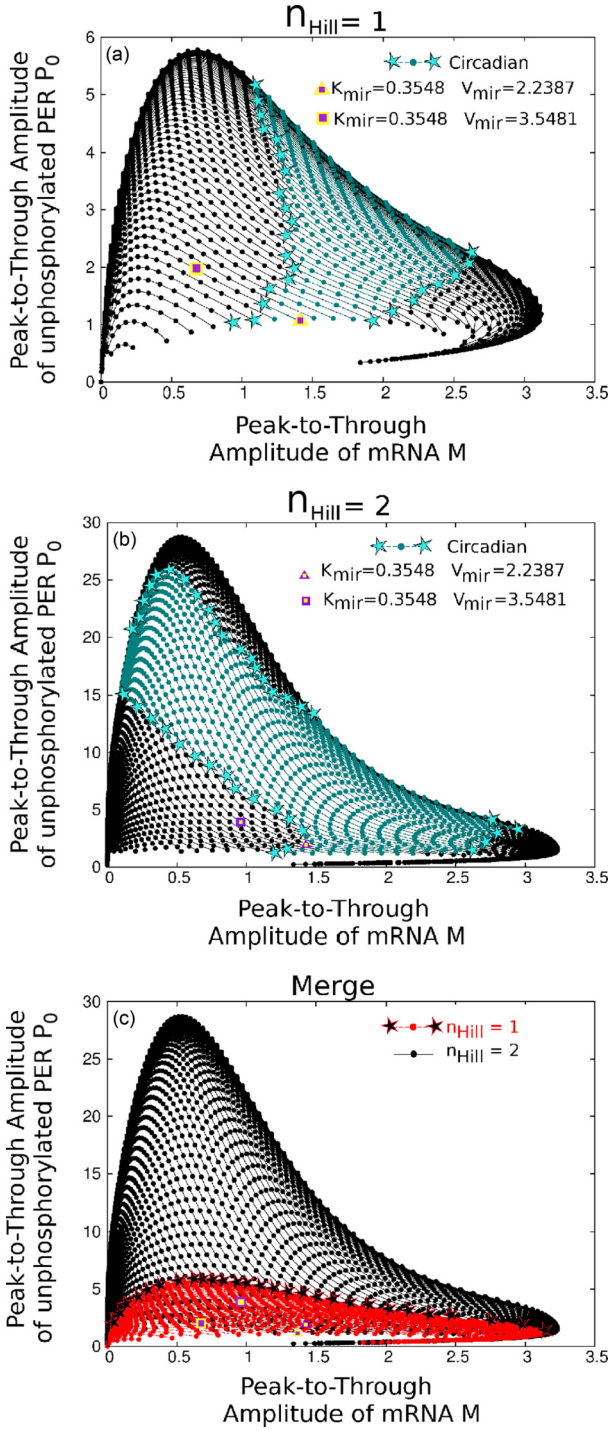

FIG. 9. The peak-to-trough amplitude for the unphosphorylated PER (P_0, y axis) is correlated with the peak-to-trough amplitude of the Per *mRNA* (M, x axis) for each pair (K_{mir}-V_{mir}) and $n_{Hill} = 1$ (a) or $n_{Hill} = 2$ (b). An increase in n_{Hill} (from 1 to 2) leads to an increase in the y-axis domain (P_0 amplitude) with almost no change in the x-axis domain (M amplitude). Concave regimes were observed for most of the V_{mir} isolines, which means that for a given V_{mir} there is a K_{mir} that maximizes the P_0/M amplitude ratio. Cyan points display the (K_{mir}-V_{mir}) pairs for which circadian periods emerge. Stars indicate the boundaries of the circadian region. Triangles and squares were used to indicate the highlighted (K_{mir}-V_{mir}) pairs showed in Fig. 8(b). (c) Superposition (merge) of panels (a) and (b). Stars indicate the boundaries of the $n_{Hill} = 1$ case.

decreases when n_{Hill} changes from 1 to 2. Summarizing, these results indicate that a moderate threshold produces a global shift of sensitivity from transcriptional repression and protein degradation to mRNA production and decay.

IV. DISCUSSION

We are interested in understanding how the dynamics of the circadian clock could be affected by the presence of a threshold in an essential process within the negative limb of the TTFL: the PER translation.

Regulation by miRNAs seems to introduce a threshold in the protein production process [23]. A molecular titration mechanism for the interaction between the miRNAs and the target mRNAs was suggested to explain these observations [21,22,24]. Here we proposed a mathematical model with a phenomenological Hill equation describing the kinetics of the PER synthesis. The Hill equation introduces a threshold on the translational process because it generates two kinetic regimes: (1) a repressed translational activity below a given mRNA concentration (threshold) and (2) a high translational activity when the threshold mRNA concentration is attained. One advantage of our modeling approach is that the sharpness of the threshold is controlled by the Hill exponent (n_{Hill}): The bigger the n_{Hill}, the stronger the *threshold effect* on the translational process. In the extreme case, $n_{Hill} \gg 1$, the translation can be thought of as an all-or-nothing process.

The numerical simulations presented here show that the emergence of oscillations within the circadian range is favored by the presence of a moderate threshold on the PER synthesis, which in our model is achieved when $n_{Hill} = 2$. The introduction of this threshold changes the relationship between periodicities and delays and produces an expansion of the protein-amplitude domain with almost no changes in the mRNA-amplitude domain.

A. Translational thresholds

Translation is a process occurring in several steps (i.e., initiation, elongation, termination, and ribosome recycling), all of which are prone to be regulated, thus allowing the modulation of gene expression in a wide range of biological situations [37]. However, translational regulation is more likely to be found during the canonical initiation step [38], and there are also other, noncanonical, mechanisms of translation initiation and regulation [39]. Two general modes of translational control were proposed [38,40,41]: (1) a global regulation through modification of initiation factors (eIFs) and secondary structures in the 5′UTR and presence of upstream open reading frame (ORFs) and (2) a mRNA-specific modulation that can be driven by regulatory protein complexes including specific RNA-binding proteins and/or micro RNAs (miRNAs). Growing evidence suggests that both modes of translational regulation can impact on the cellular circadian physiology in animals [11–13,42–48], plants [49,50], and fungi [51,52]. Thus, translational regulation adds complexity to the multilayer post-transcriptional processes involved in the cellular circadian behavior [53].

In particular, we are interested in the translational regulation of clock components [46,47,54–56], since it

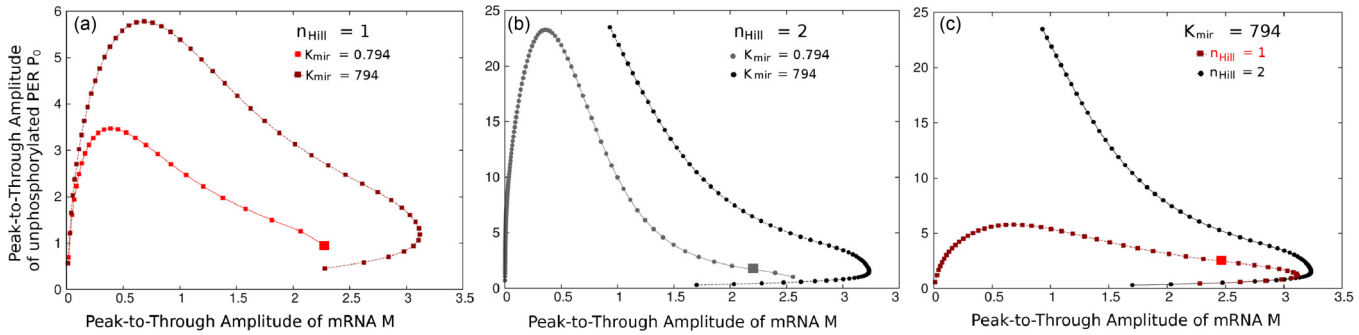

FIG. 10. Correlation between P_o and M peak-to-trough amplitudes for two $K_{\rm mir}$ values and $n_{\rm Hill} = 1$ (a) and $n_{\rm Hill} = 2$ (b). Squares indicate the $K_{\rm mir} = 0.794$ results. Independently of whether $n_{\rm Hill} = 1$ or $n_{\rm Hill} = 2$, for very high $K_{\rm mir}$ (c) and small $V_{\rm mir}$ there is a simultaneous increase of both amplitudes until the M amplitude reaches its highest value. Then, the correlation curve bends back leading to a regime where the P_0 amplitude increases while the M amplitude decreases. For $n_{\rm Hill} = 1$, the P_0 amplitude peaks and then both the M and P_0 amplitudes decrease. Square in panel (c) indicates the $n_{\rm Hill} = 1$ result.

ultimately affects the kinetics of clock protein synthesis and, as a consequence, the TTFL dynamics. The TTFL dynamics derived from different effective translational kinetics can be straightforwardly explored using mathematical modelling. In fact, we previously used this approach to understand the effects introduced by translational regulators that enhance the translational rate of PER [15]. This seems to be the function of the complex TWENTY-FOUR (TYF)–ATAXIN-2 (ATX2)–PABP in *Drosophila*, which has been recently characterized as a translation complex important for PER expression and circadian rhythms, since it activates the PER translation [11–13].

Regulation by microRNAs (miRNAs) is usually associated with both induction of mRNA destabilization (followed by decay) and translational inhibition of target mRNAs [16]. While several lines of evidence suggest that mRNA-decay comprises the major mode of miRNA-mediated repression of endogenous mRNAs [57,58], *pure* mechanisms of translational repression have been recently reported in flies, zebrafish, and humans [20]. These mechanisms are probably affecting the early step of translation initiation and can occur concurrently with different kinetics, leading to an overall increase of the silencing effect [16].

The precise molecular processes involved in *purely* (i.e., without mRNA decay) translational repression mechanisms are not fully understood, but one possibility may involve titrative miRNA-mRNA interplay. Interaction via titration mechanisms, which entails threshold-like behaviors [24], has been previously described for small RNAs and target mRNAs

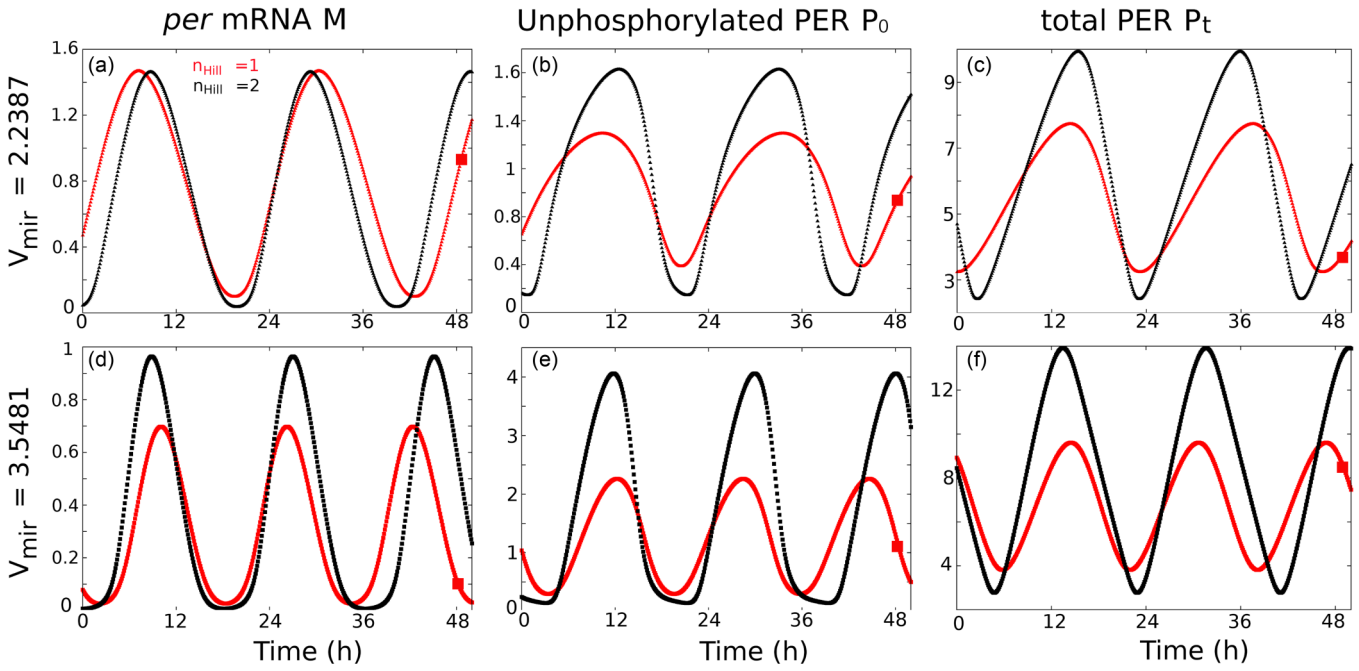

FIG. 11. Time evolution of mRNA [(a) and (d)], unphosphorylated PER [(b) and (e)], and total PER [(c) and (f)] for the $K_{\rm mir}$ isoline $= 0.3548$ and $V_{\rm mir} = 2.2387$ [(a), (b), and (c)] and $V_{\rm mir} = 3.5481$ [(d), (e), and (f)]. In red we show the results for $n_{\rm Hill} = 1$ and in black those for $n_{\rm Hill} = 2$. These time evolutions correspond to the ($K_{\rm mir}$-$V_{\rm mir}$) pairs highlighted as triangles or squares in Fig. 8(b). Squares indicate the $n_{\rm Hill} = 1$ results.

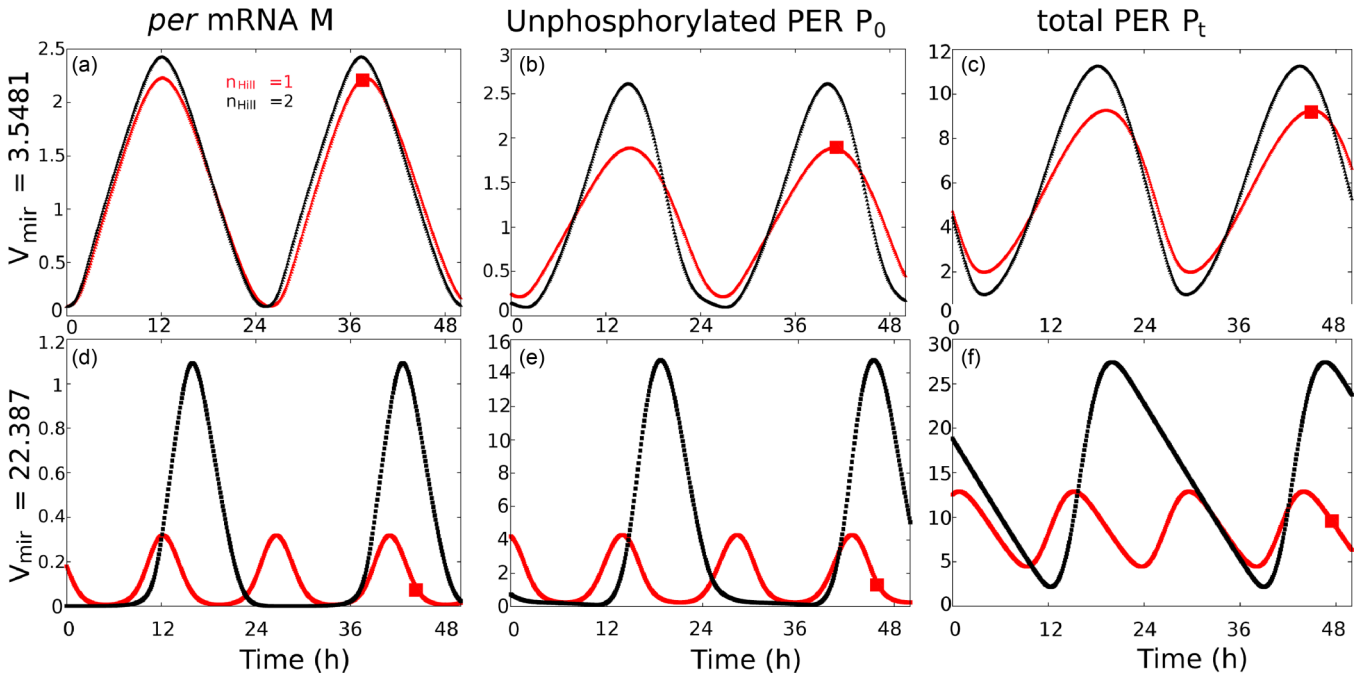

FIG. 12. Time evolution of the mRNA [(a) and (d)], unphosphorylated PER [(b) and (e)], and total PER [(c) and (f)] for the K_{mir} isoline = 1.5849 and V_{mir} =3.5481 [(a), (b), and (c)] and V_{mir} = 22.387 [(d), (e), and (f)]. The results are shown in red for $n_{Hill} = 1$ and in black for $n_{Hill} = 2$. These time evolutions correspond to the K_{mir}-V_{mir} pairs highlighted as triangles or squares in Fig. 8(e). Squares indicate the $n_{Hill} = 1$ results.

in bacteria [59] and, remarkably, a miRNA-target interaction compatible with a titration mechanism and a threshold-like behavior has been reported in mammalian cells [23,60]. Interestingly, a titrative sRNA–miRNA-mRNA interaction has been associated with indirect interactions (or cross-regulation) among target mRNAs via the shared sRNAs-miRNAs, which has been conceptualized within the competitive endogenous RNA (ceRNA) hypothesis [21,22].

Here we describe the effective kinetics of PER synthesis in terms of a Hill equation. Our choice of a Hill equation to phenomenologically represent the effects of a molecular titration mechanism was based on evidence showing that molecular titration mechanisms can generate responses that are equivalent to cooperative processes, typically described by Hill equations [29]. This modeling approach captures the main feature of a titration-based mechanism—the threshold effect. Also, this approach is simpler than explicitly considering the miRNA concentration as an additional variable (which would require an extra differential equation within our model). Besides, the Hill equation allows us to control the threshold by the n_{Hill} parameter, which does not have a *direct* molecular interpretation but describes a general miRNA-mediated threshold effect.

Since we observed that a moderate n_{Hill} increase (i.e., when n_{Hill} changes from 1 to 2) allows us to maximize the probability of finding circadian oscillations, a prediction of our model is that molecular mechanisms introducing thresholds in the effective kinetics of translation could be important to optimize the chances of emergence of circadian TTFL. Moreover, a qualitatively similar behavior is observed with a simpler Goodwin-based mathematical model (see Appendix, section "LGG1999 model," and Fig. 16), suggesting the general nature of this finding. In fact, this prediction has a solid mathematical support since the emergence of oscillations is favored by increasing nonlinearities in the TTFL model, as demonstrated in Ref. [36]. It could be interesting to experimentally determine, for instance, through synthetic biology experiments [61,62], whether mechanisms introducing thresholds in different processes facilitate the emergence of circadian oscillations. At this point it is important to note the usefulness of mathematical modeling and numerical simulation as tools to explore different molecular mechanisms underlying biological processes and as generators of new hypotheses that can be tested in the future. For instance, some exciting possibilities, supported by experimental evidence [63,64], would be to investigate (i) an oscillating miRNA effect, either in- or out-of-phase with Per mRNA expression, and (ii) a translational threshold effect acting on the expression of TTFL positive elements. These scenarios may have dramatic effects on the dynamical properties of TTFLs. In addition, our parameter sensitivity analyses show that the introduction of a moderate threshold (through $n_{Hill} = 2$) generates a global sensitivity shift of the system from transcriptional repression and protein degradation (which decrease sensitivity) to mRNA production and decay (which increase sensitivity).

B. Experimental evidences and their connection with the numerical results

As we noted, the Hill equation introduced the possibility of including thresholds in PER synthesis. Interestingly, the probability of obtaining oscillations with long periodicities (infradian rhythms) increases as the threshold in the translation becomes sharper. This result seems to be a general finding

TABLE I. Parameters

v_s	*per* mRNA transcription rate	0.5
K_i	Inhibition constant for repression of *per* mRNA transcription	2.0
n_t	Hill exponent for the repression of *per* mRNA transcription	4
K_m	Michaelis constant for *per* mRNA degradation	0.2
v_m	Maximum rate of *per* mRNA decay	0.3
V_{mir}	Maximum rate of PER synthesis	10^{-2}–10^{+6}
K_{mir}	mRNA concentration at half of the maximum translational rate	10^{-6}–10^{+3}
n_{Hill}	Hill exponent for the PER synthesis	1–50
V_1	Maximum rate of P_0 phosphorylation	6.0
K_1	Michaelis constant for P_0 phosphorylation	1.5
V_2	Maximum rate of P_1 dephosphorylation	3.0
K_2	Michaelis constant for P_1 dephosphorylation	2.0
V_3	Maximum rate of P_1 phosphorylation	6.0
K_3	Michaelis constant for P_1 phosphorylation	1.5
V_4	Maximum rate of P_2 dephosphorylation	3.0
K_4	Michaelis constant for P_2 dephosphorylation	2.0
k_1	Rate constant for entry of P_2 into the nucleus	2.0
k_2	Rate constant for exit of P_2 from the nucleus	1.0
v_d	Maximum rate of P_2 degradation	1.5
K_d	Michaelis constant for biphosphorylated P_2 degradation	0.1

since it was also observed with a simpler model (Fig. 16) and it resembles the lengthened circadian periods obtained from cultured suprachiasmatic nucleus slices in which a transient protein synthesis inhibition was chemically induced with cycloheximide [65]. Moreover, prolonged treatments with protein synthesis inhibitors are even able to stop the circadian oscillation [66]. It is well known that mutations affecting the phosporilation state and/or the stability of the TTFL negative elements can either produce arrhythmicity or lead to altered periods [67,68]. The numerical simulations presented here lend support to the proposal that translational regulation involving thresholds can be another way to tune the circadian period.

In our model the n_{Hill} parameter does not have a direct molecular interpretation. Instead, the n_{Hill} value indicates qualitatively whether a null ($n_{\text{Hill}} = 1$), moderate ($n_{\text{Hill}} > 1$), or sharp ($n_{\text{Hill}} \gg 1$) miRNA-mediated threshold effect is present in PER synthesis. Since we have mainly focused our analysis on the comparison between $n_{\text{Hill}} = 1$ and $n_{\text{Hill}} = 2$, we have interpreted these two conditions as indicating the absence or presence of a miRNAs effect, respectively.

In order to validate our model, we searched the literature for experimental evidence comparing the oscillatory features of the TTFL in the presence and absence of miRNA activity. We found that this approach has been used to evaluate the impact of global miRNA regulation on the mammalian molecular clock [69,70]. These papers provide experimental support for the idea that miRNAs are involved as an additional layer of post-transcriptional regulation for the fine tuning of circadian rhythms rather than be essential components of the molecular core clock.

Although it is not possible to completely rule out the role of pleiotropic effects indirectly influencing the clock dynamics, either by deleting the pre-miRNA processing enzyme Dicer in mouse embryonic fibroblasts (MEFs) [69] or by using liver explants derived from the Dicer knockout (KO) mice [70], these authors present several pieces of evidence strongly suggesting a direct effect of miRNA over the *Per1* and *Per2* translation.

These studies showed, however, different results with regards to the oscillatory features of the TTFL. On one hand, in liver explants the miRNAs activity seems to

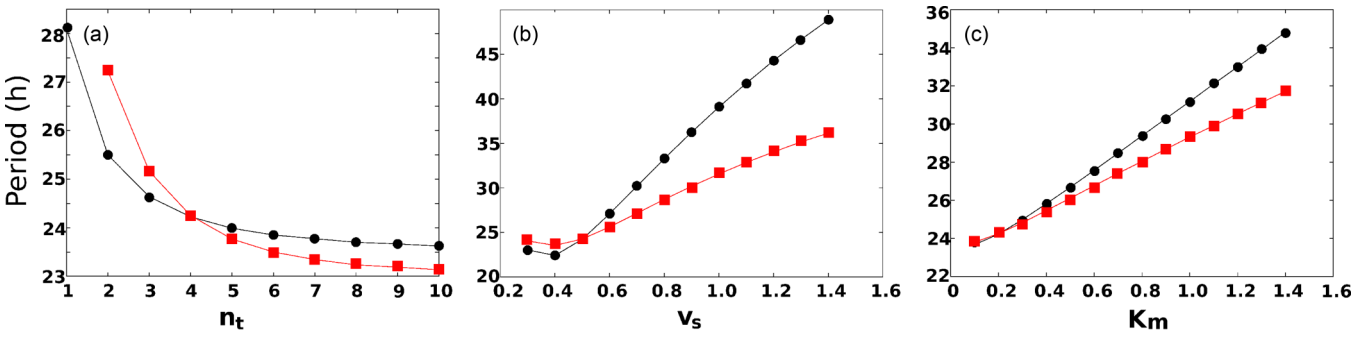

FIG. 13. Period sensitivity to changes in parameters related to mRNA production and decay: (a) The Hill exponent for the repression of mRNA transcription, n_t; (b) the maximum rate of per mRNA synthesis, v_s; and (c) the Michaelis constant for mRNA degradation, K_m. Results are shown for $n_{\text{Hill}} = 1$ (red squares) and $n_{\text{Hill}} = 2$ (black circles).

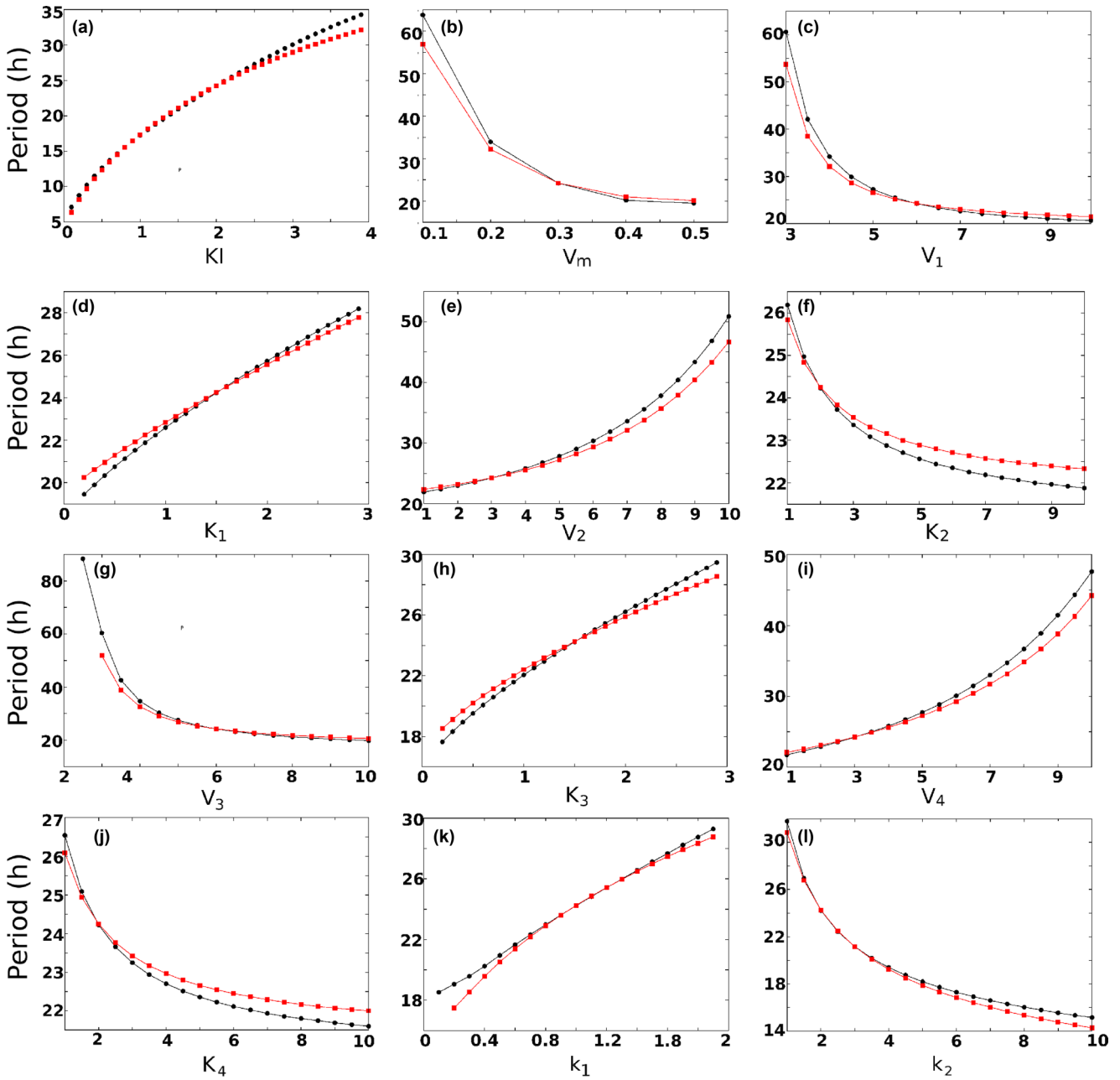

FIG. 14. Period sensitivity to nontranslation-related model parameters. Inhibition constant for repression of Per mRNA transcription, K_i (a); maximum rate of Per mRNA decay, v_m, (b); maximum rate of unphosphorylated PER phosphorylation, V_1, (c); Michaelis constant for unphosphorylated PER phosphorylation, K_1, (d); maximum rate of monophosphorylated PER dephosphorylation, V_2, (e); Michaelis constant for monophosphorylated PER dephosphorylation, K_2, (f); maximum rate of monophosphorylated PER phosphorylation, V_3, (g); Michaelis constant for monophosphorylated PER phosphorylation, K_3, (h); maximum rate of biphosphorylated PER dephosphorylation, V_4, (i); Michaelis constant for biphosphorylated PER dephosphorylation, K_4, (j); rate constant for exit of biphosphorylated PER from the nucleus, k_2, (k); rate constant for entry of biphosphorylated PER into the nucleus, k_1, (l). Red squares and black circles correspond to translation kinetics with $n_{\mathrm{Hill}} = 1$ and $n_{\mathrm{Hill}} = 2$, respectively. Period profiles did not exhibit significant changes between these two conditions.

moderately shorten the period of the molecular clock, since Dicer KO explants tend to exhibit longer periods than those derived from wild-type (WT) mice [70]. In addition, the miRNAs activity in liver also seems to produce a shortening of the time delays, since the upswing of the PER2::LUC bioluminescence rhythms was shortened in the WT liver explants as compared to Dicer KO explants. On the other hand, in MEFs the miRNAs activity seems to contribute to the lengthening of the circadian period, since control MEF's exhibited longer periods than Dicer-deleted MEF's [69]. These experiments also suggested that miRNAs activity introduces time delays by direct inhibition of PER accumulation in the cytoplasm [69]. From an experimental point of view, the differences between MEF's and liver results were related to tissue specificities in miRNA function [70].

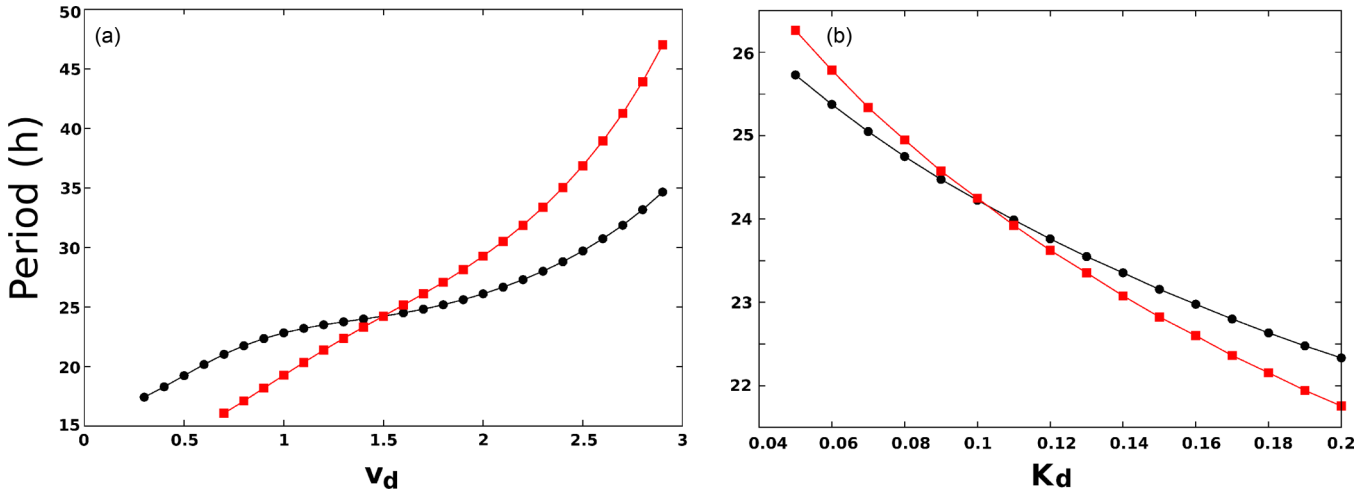

FIG. 15. Period sensitivity to changes in parameters related to protein degradation: (a) The maximum rate of PER degradation, v_d, and (b) the Michaelis constant for PER degradation, K_d. Results are shown for $n_{\mathrm{Hill}} = 1$ (red squares) and $n_{\mathrm{Hill}} = 2$ (black circles).

Since Dicer depletion leads to the absence of mature miRNAs, and therefore to the absence of a miRNA-mediated effect, we interpret this situation as being similar to the condition $n_{\mathrm{Hill}} = 1$ in our model. Analogously, results derived from the controls, where miRNAs are active, can be interpreted in our model as following from the condition $n_{\mathrm{Hill}} > 1$. This interpretation allows us to make some qualitative comparisons between our theoretical results and the results derived from these experimental studies.

First, consistently with the results from liver [70], we showed that some V_{mir} conditions in our model generated TTFL's period and delay shortenings when n_{Hill} changed from 1 (similar to the DICER KO condition: absence of miRNA activity) to $n_{\mathrm{Hill}} = 2$ (similarly to the WT condition: presence of miRNA activity). Interestingly, these V_{mir} values also produced delays between 6 and 8 h and periods between 20 and 28 h (inside the violet rectangle of Fig. 8), which are the ranges previously reported [30–35,71]. Under other V_{mir} conditions, our model yields a diversity of behaviors among which we can find the situation reported in MEF's in Ref. [69]: TTFL period and delay lengthenings. However, in this case, even after time delays were introduced (by increasing the n_{Hill} parameter from 1 to 2) the resulting delays are short (about 4–6 h) in comparison to those previously reported [34,35,71]. Thus, by only assuming a moderate miRNA-mediated threshold in PER synthesis, our model is able to reproduce the changes in period and delay reported in both liver and MEF's Dicer KO experiments, providing a framework that conciliates these experimental observations. Indeed, when we increase n_{Hill} from 1 to 2 in a simpler but similar TTFL mathematical

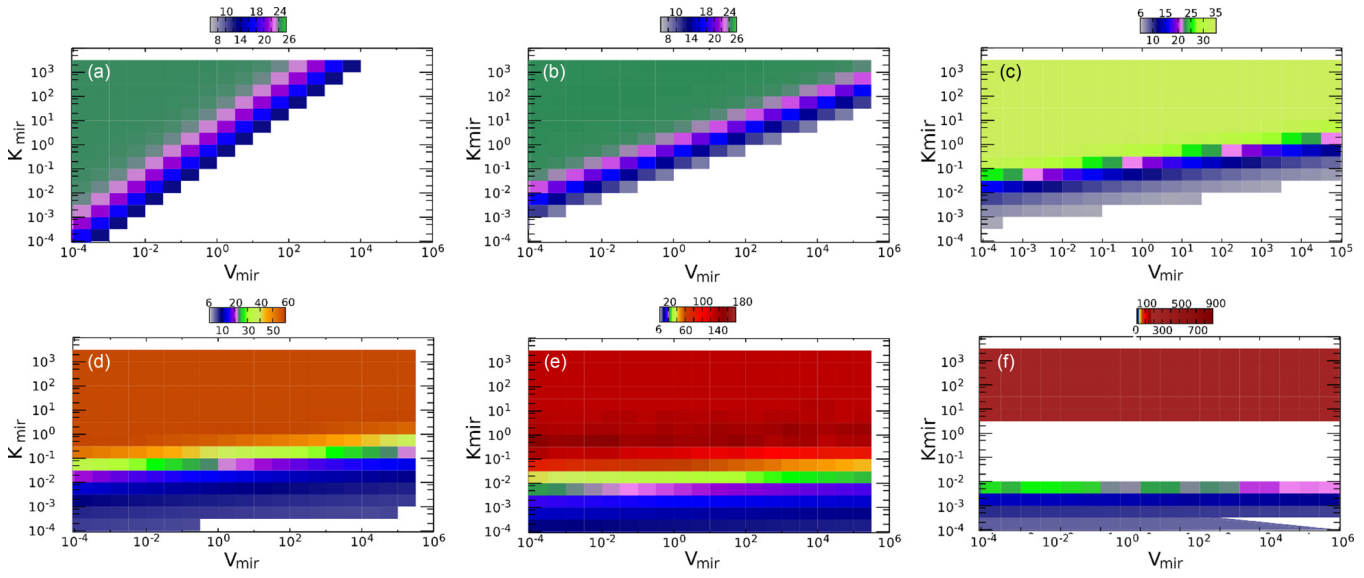

FIG. 16. Phase diagrams in the V_{mir}-K_{mir} subspace obtained with the LGG199 model for $n_{\mathrm{Hill}} = 1$ (a), 2 (b), 5 (c), 10 (d), 20 (e), and 50 (f) obtained with the LGG199 model. Pseudocolor indicates the K_{mir}-V_{mir} pairs for which a periodic solution is obtained. The period length (τ) is shown in each key and increases from the bottom up. White regions indicate K_{mir}-V_{mir} pairs that do not correspond to an oscillatory solution for the system. Axes are in logarithmic scale, which allows us to observe details at small K_{mir}-V_{mir} values.

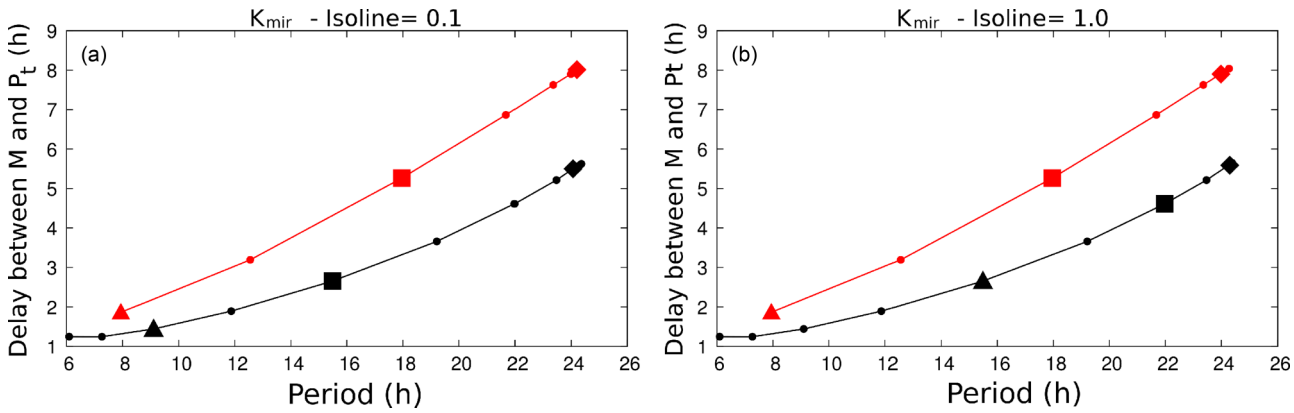

FIG. 17. Individual K_{mir} isolines for $n_{\mathrm{Hill}} = 1$ (red line and points, top) and $n_{\mathrm{Hill}} = 2$ (black line and points, bottom) when K_{mir} was fixed at $K_{\mathrm{mir}} = 0.1$ (a) or $K_{\mathrm{mir}} = 1$ (b) in the LGG1999 model. Pairs of triangles, squares, and diamonds correspond to the same V_{mir} values in each K_{mir} isoline.

model (see Appendix, section "LGG1999 model," and Fig. 17) we find that a mild threshold also produces diverse changes in the delay-period relationship (i.e., delay and period lengthening, period lengthening with delay shortening, delay and period shortening). This feature is mainly determined by the specific value of V_{mir}. Importantly, we observed TTFL's period and delay shortenings when n_{Hill} changed from 1 to $n_{\mathrm{Hill}} = 2$ [red to black squares and red to black diamonds in Fig. 17(a)] and some of these V_{mir} values also lead to circadian periods with delays between 6 and 8 h [for example, red to black diamonds in Fig. 17(a)]. Moreover, we also find V_{mir} values producing oscillations with short delays (about 4–6 h) for which a n_{Hill} change from 1 to 2 leads to TTFL period and delay lengthenings [for example, red to black triangles in Fig. 17(b)], similarly to the findings showed in Fig. 8 (squares). Therefore, these seems to be general findings, supporting two predictions of our model: (i) The observed tissue differences may be related to translational enhancers involved in the PER synthesis (associated with V_{mir}) and (ii) delays in MEF's may be shorter than in liver. It is worth noting, however, that the comparison of our main results with those emerging from the simpler TTFL mathematical model (Appendix, section "LGG1999 model") also highlighted those effects that were produced by the interaction between the nonlinearities describing the different kinetic processes. This is therefore a useful approach for structurally analyzing to what extent the processes relate to each other and we will explore it in depth in the future.

Second, the PER2::LUC free-running rhythms measured from liver explants of Dicer knockout animals (analogously to the $n_{\mathrm{Hill}} = 1$ in our model) exhibit a less-steep upswing slope than controls (analogously to the $n_{\mathrm{Hill}} = 2$ in our model) [70]. Similarly, the introduction of the threshold in translation changes the functional waveforms. Specifically, an increase of n_{Hill} produces a flattening of the P_0 troughs, which introduces time delays since it takes a longer time to trigger the upswing phase of the protein dynamics. The same feature is observed as V_{mir} increases. In addition, the slope of the upswing phase becomes steeper as n_{Hill} increases, which is another qualitative similarity between the experiments and our model and seems to affect the time delays, because it determines the rate of P_0 accumulation. Therefore, the balance of these two effects is probably influencing the period and delay lengths.

Third, the PER2::LUC peak-to-trough amplitude in both MEF's and liver increased in the presence of miRNA activity. Consistently, we also observed an increase of PER peak-to-trough amplitude when $n_{\mathrm{Hill}} > 1$. Nevertheless, the stationary PER1 and PER2 protein levels were systematically higher throughout the day in Dicer mutants (in MEF's and liver) as compared with controls. In our simulations, this observation is true only at the troughs but not at the peaks. We think that this difference between the experiments and our simulations is associated with the previously discussed miRNA-mediated destabilization and decay of target mRNAs, which are likely to be present in these experiments. Indeed, it was recently found that the *Per2* mRNA 3′UTR has binding sites for miR-24 and miR-30, which contribute to increase *Per2* mRNA destabilization [17]. This effect is likely to be abolished in Dicer KO, yielding systematically high stationary PER's levels. Qualitatively similar are the results of a mathematical model developed by Nandi and collaborators [18]. In that model they studied a scenario in which miRNAs can effectively increase the mRNA degradation rate and thereby shorten the *Per* mRNA half-life. They found that the introduction of miRNA drastically reduces the amplitude of protein oscillations and shortens the circadian period. So a combination of miRNA-mediated mRNA destabilization and translational regulation may explain the circadian amplitude profile.

In summary, miRNAs have important and diverse roles in circadian clock regulation; the mechanism by which they exert their function may include a combination of mRNA destabilization and translational regulation. These may depend on tissue specificities, mice strain, and light regimen (environmental or experimental conditions) [72]. By assuming a moderate miRNA-mediated threshold in PER synthesis, our model allows us to explain previous experimental observations related to the translational regulation of negative elements in the TTFL. We provide new elements for thinking of the translational threshold as a mechanism that favors the emergence of circadian rhythmicity, tuning the delays and the cell capacity to control the protein amplitude domain with almost negligible changes in the mRNA domain.

ACKNOWLEDGMENTS

We thank Dr. Lucas Valdez for useful discussions. This work was supported by SECyT-UNC (Project No. 05-B457) and CONICET (PIP 11220150100644), Argentina.

APPENDIX

1. The TTFL model

The conceptual molecular clock model shown in Fig. 1(a) can be transformed into a mathematical model by the selection of adequate mathematical equations and parameter values in order to represent the biochemical processes involved [27]. Since the exact functional forms of each process are not experimentally known, the model relies on the following assumptions:

(1) The *per* mRNA (M) is transcribed in the nucleus and transferred to the cytoplasm at a rate v_s (nM h^{-1}), where it decays in a Michaelis-Menten fashion with rate v_m (nM h^{-1}) and Michaelis constant K_m (nM).

(2) In the cytoplasm, the *per* mRNA can be translated to produce the PER protein. In previous models the PER translation rate was assumed to be proportional to the *per* mRNA concentration and characterized by the first-order rate constant k_s (h^{-1}), [18,25,26]. Here we assumed that a Hill equation represents the rate of PER synthesis based on the following considerations:

(a) It is well known that multiple regulators and factors are involved in the effective kinetics of protein synthesis, and therefore it is likely that this process occurs with nonlinear kinetics [73,74].

(b) PER translation is modulated by regulators that enhance the PER translation [11,13,14,45]. In our previous work [15] we have interpreted the global effect of such regulators as enzymatic catalyzers that enhance the translational rate and impose a maximum velocity of reaction achieved at saturating mRNA concentration. A Michaelis-Menten kinetics was proposed to represent these features.

(c) In the last few years an increasing amount of evidence has suggested that microRNAs (miRNAs) regulate several aspects of circadian clock function [75], and in particular, that the mRNA of *Per1* and *Per2* are targets of miRNA function, [69,70].

(d) The way in which some miRNAs interact with their targets can be described in terms of a titration mechanism, characterized by a threshold effect, hypersensitivity of the system around the threshold, and cross-talk among miRNAs-targets. This kind of miRNA-mediated translational regulation, then, establishes a threshold level of target mRNA below which protein production is highly repressed, [23,24,76].

Molecular titration mechanisms can generate responses that are equivalent to cooperative processes [29]. Therefore, we propose a Hill equation [Eq. (2)] to *phenomenologically* model a miRNA-mediated thresholding in PER synthesis. By taking into account a Hill kinetics for PER translation, we have incorporated three parameters to the model: the K_{mir} (nM) constant; the maximum rate of the translational process V_{mir} (nM h^{-1}) and the the Hill exponent (n_{Hill}). As noted under Methods, V_{mir} is the parameter that controls the maximum PER translation rate, biologically interpreted as being proportional to the concentration of multiple translational enhancers involved in the PER synthesis; K_{mir} is the parameter that indicates the mRNA concentration at which the PER synthesis is one half of its maximum rate, and the Hill exponent, (n_{Hill}), is the parameter that controls the sharpness of the translational threshold. It indicates qualitatively whether a null ($n_{\mathrm{Hill}} = 1$), moderate ($n_{\mathrm{Hill}} > 1$) or sharp ($n_{\mathrm{Hill}} \gg 1$) miRNA-mediated threshold effect is present in PER synthesis. When $n_{\mathrm{Hill}} = 1$ the Hill equation becomes a Michaelis-Menten equation [15]. When $n_{\mathrm{Hill}} \gg 1$ (i.e., $n_{\mathrm{Hill}} = 50$), the translation can be thought of as an all-or-nothing process, which may seem biologically unrealistic, but we have included it in some of our simulations since analyzing extreme cases may be useful to identify some tendencies that are not so evidently expressed at low values of n_{Hill}. Nevertheless, we have mainly focused our analysis on the comparison between $n_{\mathrm{Hill}} = 1$ and $n_{\mathrm{Hill}} = 2$, and we have interpreted these two conditions as absence or presence of a moderate miRNAs threshold effect, respectively.

(3) The unphosphorylated PER (P_0) is phosphorylated twice in a consecutive and reversible fashion, resulting in the monophosphorylated PER (P_1) and the biphosphorylated PER (P_2). The first phosphorylation-dephosphorylation step is modeled by a Michaelis-Menten mechanism with a maximum rate V_1 (nM h^{-1}) and a Michaelis constant K_1 (nM) for the forward reaction and with a maximum rate V_2 (nM h^{-1}) and a Michaelis constant K_2 (nM) for the reverse reaction. The same kinetics is assumed for the second phosphorylation-dephosphorylation step, with maximum rates V_3 (nM h^{-1}) and V_4 (nM h^{-1}), and Michaelis constants K_3 (nM h^{-1}) and K_4 (nM h^{-1}), respectively.

(4) Only biphosphorylated PER (P_2) can be degraded with a Michaelis-Menten kinetics with maximum rate v_d (nM h^{-1}) and Michaelis constant K_d (nM).

(5) Nuclear translocation of the biphosphorylated PER is considered as a reversible step with first-order rate constants k_1 (h^{-1}) and k_2 (h^{-1}) for the forward and reverse processes, respectively.

(6) To simplify the model it was assumed that nuclear PER (P_n) itself is the repressor exerting the negative feedback on *per* expression. The feedback term is described by a Hill-like equation with Hill exponent n_t. The bigger the n_t value, the more cooperative is the repression of *per* transcription. A study about the effect of n_t was included in our previous work [15]. Here we assumed $n_t = 4$, which is consistent with the idea that repression must be a cooperative process [77].

Summarizing, the model consists of a set of five ordinary differential equations describing the time evolution of five components of the molecular circadian clock: M, P_0, P_1, P_2, and P_n. The system requires 20 parameters, whose definitions and values are listed in Table I and are the same as those reported in Ref. [26].

It is worth noting that this model has an intermediate complexity (5 variables and 20 parameters), but other more simplistic or complex (detailed) models have also been proposed to study different aspects of TTFL dynamics, [78–82]. Very detailed models may be helpful to establish direct comparisons with experimental data at the expense of their predictive capacity. Indeed, increasing the number of variables and parameters does not significantly improve the description

TABLE II. Parameters of the LGG1999 model

v_s	*per* mRNA transcription rate	1.6
K_i	Inhibition constant for repression of *per* mRNA transcription	1.0
n_t	Hill exponent for the repression of *per* mRNA transcription	4
K_m	Michaelis constant for *per* mRNA degradation	0.5
v_m	Maximum rate of *per* mRNA decay	0.505
V_{mir}	Maximum rate of PER synthesis	10^{-4}–10^{+6}
K_{mir}	mRNA concentration at half of the maximum translational rate	10^{-4}–10^{+3}
n_{Hill}	Hill exponent for the PER synthesis	1–50
k_1	Rate constant for entry of P_2 into the nucleus	0.5
k_2	Rate constant for exit of P_2 from the nucleus	0.6
v_d	Maximum rate of P_2 degradation	1.4
K_d	Michaelis constant for biphosphorylated P_2 degradation	0.13

of the basic properties of a TTFL. Instead, it obscures the mathematical and computational analysis because many of the parameters have unknown experimental values.

Units: K_i, K_m, K_1, K_2, K_3, K_4, K_d, and K_{mir} are in nM; v_s, v_m, V_1, V_2, V_3, V_4, v_d, and V_{mir} are in nM h^{-1}; k_1 and k_2 are in h^{-1}.

2. LGG1999 model

We implemented the Hill translation kinetics in a simpler Goodwin-based model, previously described by Leloup, Gonze, and Goldbeter [25]. This model, which we call LGG1999, is quite similar to the one we chose for the present article, except for the specific parameter values (listed in Table II) and the two reversible phosphorylation processes, absent in this simpler version. The differential equations are

$$\frac{dM}{dt} = v_s \frac{K_i^{n_t}}{K_i^{n_t} + P_n^{n_t}} - v_m \frac{M}{K_m + M}, \tag{A1}$$

$$\frac{dP_0}{dt} = V_{\mathrm{mir}} \frac{M^{n\mathrm{Hill}}}{K_{\mathrm{mir}}^{n\mathrm{Hill}} + M^{n\mathrm{Hill}}} - v_d \frac{P_0}{K_d + P_0} - k_1 P_0 + k_2 P_n, \tag{A2}$$

$$\frac{dP_n}{dt} = k_1 P_0 - k_2 P_n. \tag{A3}$$

Thus, the LGG1999 model contains only three differential equations, which resemble the original Goodwin model and its more precise Griffith implementation [83,84]. The differences are related to the mRNA and protein degradation kinetics: While in the LGG1999 model we described them by Michaelis-Menten functions, in the Goodwin and Griffith they were assumed to have first-order kinetics. In order to test the generality of the results shown in Fig. 2, we explored numerically the translational parameter space defined by V_{mir}, K_{mir} and n_{Hill} and found that the oscillatory (colored) region within the translational parameter space increases when $n_{\mathrm{Hill}} > 1$ (Fig. 16). This result is qualitatively similar to that shown in in the Fig. 2. Circadian periodicity is also favored by a moderate increase of n_{Hill}.

In addition, we tested the generality of the delay-period relationships described in Figs. 5 and 8. Figure 17 shows the comparison between representative K_{mir} isolines for $n_{\mathrm{Hill}} = 1$ and $n_{\mathrm{Hill}} = 2$ obtained with the LGG1999 model. When we compare this result with Fig. 8, we recognize similarities and differences. The main similarities are related to the delay-period relationship, which is strongly dependent on V_{mir}. It presents a diversity of behaviors when going from $n_{\mathrm{Hill}} = 1$ to $n_{\mathrm{Hill}} = 2$: delay and period lengthening [red and black triangles in Fig. 17(b)]; period lengthening with delay shortening [red and black squares in Fig. 17(b)] and delay and period shortening [red and black squares and diamonds in Fig. 17(a)]. The main difference we observe is that the LGG199 model does not yield *twisted* isolines, such as those observed in Fig. 8. Instead, the delays are monotonic functions of the period length for the whole delay and period range. Indeed, the delay-period relationships found with the LGG199 model exhibit a steeper slope for $n_{\mathrm{Hill}} = 1$ than for $n_{\mathrm{Hill}} = 2$, while the opposite effect is observed in the almost linear delay-period relationship region of Fig. 5(f) (i.e., within the violet rectangle of Fig. 8). Therefore, the LGG199 model presents less period robustness for $n_{\mathrm{Hill}} = 2$ than for $n_{\mathrm{Hill}} = 1$. In addition, the range of periodicities found with the LGG199 model never extends beyond 25 h. On the contrary, in Fig. 8 the periodicities extend to more than 30 h. These differences are likely to be related to the interaction between the two reversible phosphorylation processes (absent in the LGG199 model) and the mild threshold introduced in the translation process. Certainly, all these aspects could be better explored in future works.

Units: K_i, K_m, K_d, and K_{mir} are in nM; v_s, v_m, v_d, and V_{mir} are in nM h^{-1}; k_1 and k_2 are in h^{-1}.

[1] H. Daido, Phys. Rev. Lett. **87**, 048101 (2001).
[2] N. Mosheiff, B. M. C. Martins, S. Pearl-Mizrahi, A. Grünberger, S. Helfrich, I. Mihalcescu, D. Kohlheyer, J. C. W. Locke, L. Glass, and N. Q. Balaban, Phys. Rev. X **8**, 021035 (2018).
[3] J. M. Hurley, J. J. Loros, and J. C. Dunlap, Trends Biochem. Sci. **41**, 834 (2018).
[4] L. Fuhr, M. Abreu, P. Pett, and A. Relógio, Comput. Struct. Biotechnol. J. **13**, 417 (2015).

[5] T. S. Hatakeyama and K. Kaneko, Phys. Rev. Lett. **115**, 218101 (2015).
[6] J. S. Takahashi, Nat. Rev. Genet. **18**, 164 (2017).
[7] E. Garbarino-Pico and C. B. Green, Cold Spring Harb. Symp. Quant. Biol. **72**, 145 (2007).
[8] E. Garbarino-Pico, P. Nieto, and M. Guido, in *Circadian Rhythms: Biology, Cognition and Disorders*, *Human Anatomy and Physiology*, edited by L. Golovkin and A. Maliszkewicz (Nova Science Publishers, Inc., Hauppauge, NY, 2011), p. 247.
[9] A. Chaix, A. Zarrinpar, and S. Panda, J. Cell Biol. **215**, 15 (2016).
[10] L. Mendoza-Viveros, P. Bouchard-Cannon, S. Hegazi, A. H. Cheng, S. Pastore, and H.-Y. M. Cheng, Cell. Molec. Life Sci. **74**, 1035 (2017).
[11] C. Lim, J. Lee, C. Choi, V. L. Kilman, J. Kim, S. M. Park, S. K. Jang, R. Allada, and J. Choe, Nature **470**, 399 (2011).
[12] C. Lim and R. Allada, Science **340**, 875 (2013).
[13] Y. Zhang, J. Ling, C. Yuan, R. Dubruille, and P. Emery, Science **340**, 879 (2013).
[14] Y. Liu, W. Hu, Y. Murakawa, J. Yin, G. Wang, M. Landthaler, and J. Yan, Sci. Rep. **3**, 2054 (2013).
[15] P. S. Nieto, J. A. Revelli, E. Garbarino-Pico, C. A. Condat, M. E. Guido, and F. A. Tamarit, PLoS One **10**, 1 (2015).
[16] H. oki Iwakawa and Y. Tomari, Trends Cell Biol. **25**, 651 (2015).
[17] S. H. Yoo, S. Kojima, K. Shimomura, N. Koike, E. D. Buhr, T. Furukawa, C. H. Ko, G. Gloston, C. Ayoub, K. Nohara, B. A. Reyes, Y. Tsuchiya, O. J. Yoo, K. Yagita, C. Lee, Z. Chen, S. Yamazaki, C. B. Green, and J. S. Takahashi, Proc. Natl. Acad. Sci. USA **114**, E8855 (2017).
[18] A. Nandi, C. Vaz, A. Bhattacharya, and R. Ramaswamy, BMC Syst. Biol. **3**, 45 (2009).
[19] K. Liu and R. Wang, J. Theor. Biol. **304**, 103 (2012).
[20] A. Fukao, T. Aoyama, and T. Fujiwara, RNA Biol. **12**, 922 (2015).
[21] L. Salmena, L. Poliseno, Y. Tay, K. Lev, and P. Pandolfi, Cell **146**, 353 (2011).
[22] Y. Tay, J. Rinn, and P. Pandolfi, Nature **505**, 344 (2014).
[23] S. Mukherji, M. S. Ebert, G. X. Y. Zheng, J. S. Tsang, P. A. Sharp, and A. van Oudenaarden, Nat. Genet. **43**, 854 (2011).
[24] C. Bosia, A. Pagnani, and R. Zecchina, PLoS One **8**, 1 (2013).
[25] A. Goldbeter, Proc. R. Soc. Lond. B: Biol. Sci. **261**, 319 (1995).
[26] D. Gonze, J. Halloy, and A. Goldbeter, Proc. Natl. Acad. Sci. USA. **99**, 673 (2002).
[27] D. G. Beersma, J. Biol. Rhy. **20**, 304 (2005).
[28] C. H. Dibner, D. Sage, M. Unser, C. Bauer, T. d'Eysmond, F. Naef, and U. Schibler, EMBO J. **28**, 123 (2009).
[29] N. E. Buchler and M. Louis, J. Mol. Biol **384**, 1106 (2008).
[30] E. Nagoshi, C. Saini, C. Bauer, T. Laroche, F. Naef, and U. Schibler, Cell **119**, 693 (2012).
[31] J. D. Plautz, M. Straume, R. Stanewsky, C. F. Jamison, C. Brandes, H. B. Dowse, J. C. Hall, and S. A. Kay, J. Biol. Rhy. **12**, 204 (1997).
[32] S. J. Aton, J. E. Huettner, M. Straume, and E. D. Herzog, Proc. Natl. Acad. Sci. USA **103**, 19188 (2006).
[33] E. D. Herzog, S. J. Aton, R. Numano, Y. Sakaki, and H. Tei, J. Biol. Rhy. **19**, 35 (2004).
[34] W. So and M. Rosbash, EMBO J. **16**, 7146 (1997).
[35] A. Korencic, G. Bordyugov, R. Kosir, D. Rozman, M. Golisnik, and H. Herzel, PLoS One **7**, 1 (2012).
[36] G. Kurosawa, A. Mochizuki, and Y. Iwasa, J. Theor. Biol. **216**, 193 (2002).
[37] N. Robichaud and N. Sonenberg, Curr. Opin. Biotechnol. **45**, 102 (2017).
[38] A. G. Hinnebusch, I. P. Ivanov, and N. Sonenberg, Science **352**, 1413 (2016).
[39] R. Lacerda, J. Menezes, and L. Romão, Cell. Mol. Life Sci. **74**, 1659 (2017).
[40] N. Sonenberg and A. G. Hinnebusc, Cell **136**, 731 (2009).
[41] F. Gebauer and M. W. Hentze, Nat. Rev. Mol. Cell Biol. **5**, 827 (2004).
[42] Y. Huang, J. A. Ainsley, L. G. Reijmers, and F. R. Jackson, PLoS Biol. **11**, e1001703 (2013).
[43] Y. Huang, G. P. McNeil, and F. R. Jackson, PLoS Genet. **10**, e1004536 (2014).
[44] C. Jouffe, G. Cretenet, L. Symul, E. Martin, F. Atger, F. Naef, and F. Gachon, PLoS Biol. **11**, 1 (2013).
[45] S. Bradley, S. Narayanan, and M. Rosbash, Genetics **192**, 943 (2012).
[46] S. Kojima, K. Matsumoto, M. Hirose, M. Shimada, M. Nagano, Y. Shigeyoshi, S.-i. Hoshino, K. Ui-Tei, K. Saigo, C. B. Green, Y. Sakaki, and H. Tei, Proc. Natl. Acad. Sci. USA **104**, 1859 (2007).
[47] K.-H. Lee, K.-C. Woo, D.-Y. Kim, T.-D. Kim, J. Shin, S. M. Park, S. K. Jang, and K.-T. Kim, Moll. Cell. Biol. **32**, 717 (2012).
[48] J. Lipton, E. Yuan, L. Boyle, D. Ebrahimi-Fakhari, E. Kwiatkowski, A. Nathan, T. Güttler, F. Davis, J. Asara, and M. Sahin, Cell **161**, 1138 (2015).
[49] A. Missra, B. Ernest, T. Lohoff, Q. Jia, J. Satterlee, K. Ke, and A. G. von Arnim, Plant Cell **27**, 2582 (2015).
[50] A. Romanowski and M. J. Yanovsky, Front. Plant Sci. **6**, 437 (2015).
[51] K. Lee, J. J. Loros, and J. C. Dunlap, Science **289**, 107 (2000).
[52] S. Z. Caster, K. Castillo, M. S. Sachs, and D. Bell-Pedersen, Proc. Natl. Acad. Sci. USA **113**, 9605 (2016).
[53] S. Kojima, D. L. Shingle, and C. B. Green, J. Cell Sci. **124**, 311 (2011).
[54] Y. Fujimoto, K. Yagita, and H. Okamura, Genes Cells **11**, 525 (2006).
[55] K. Nishii, I. Yamanaka, M. Yasuda, Y. B. Kiyohara, Y. Kitayama, T. Kondo, and K. Yagita, Neurosci. Lett. **401**, 44 (2006).
[56] Y. Yamamoto, K. Yagita, and H. Okamura, Mol. Cell. Biol. **25**, 1912 (2005).
[57] S. Eichhorn, H. Guo, S. McGeary, R. Rodriguez-Mias, C. Shin, D. Baek, S. hao Hsu, K. Ghoshal, J. Villen, and D. Bartel, Mol. Cell **56**, 104 (2014).
[58] E. Huntzinger and E. Izaurralde, Nat. Rev. Genet. **12**, 99 (2011).
[59] E. Levine, Z. Zhang, T. Kuhlman, and T. Hwa, PLoS Biol. **5**, 1 (2007).
[60] C. Bosia, F. Sgrò, L. Conti, C. Baldassi, D. Brusa, F. Cavallo, F. DiCunto, E. Turco, A. Pagnani, and R. Zecchina, Genome Biol. **18**, 37 (2017).
[61] M. Tigges, T. T. Marquez-Lago, J. Stelling, and M. Fussenegger, Nature **457**, 309 (2009).
[62] S. Auslander and M. Fussenegger, Curr. Opin. Biotechnol. **48**, 54 (2017).

[63] Y. Xue and Y. Zhang, BMC Neurosci **19**, 1 (2018).
[64] H.-Y. M. Cheng, J. W. Papp, O. Varlamova, H. Dziema, B. Russell, J. P. Curfman, T. Nakazawa, K. Shimizu, H. Okamura, S. Impey, and K. Obrietan, Neuron **54**, 813 (2007).
[65] S.-y. Nishide, D. Ono, Y. Yamada, S. Honma, and K.-i. Honma, Eur. J. Neurosci. **35**, 291.
[66] S. B. Khalsa, D. Whitmore, and G. D. Block, Proc. Natl. Acad. Sci. USA **89**, 10862 (1992).
[67] L. F. Larrondo, C. Olivares-Yañez, C. L. Baker, J. J. Loros, and J. C. Dunlap, Science **347** (2015).
[68] E. S. Maywood, J. E. Chesham, Q.-J. Meng, P. M. Nolan, A. S. I. Loudon, and M. H. Hastings, J. Neurosci. **31**, 1539 (2011).
[69] R. Chen, M. D'Alessandro, and C. Lee, Curr. Biol. **23**, 1959 (2013).
[70] N.-H. Du, A. B. Arpat, M. De Matos, and D. Gatfield, eLife **3**, e02510 (2014).
[71] R. Stanewsky, K. S. Lynch, C. Brandes, and J. C. Hall, J. Biol. Rhy. **17**, 293 (2002).
[72] S. Kiessling, A. Ucar, K. Chowdhury, H. Oster, and G. Eichele, PLoS ONE **12**, e0176547 (2017).
[73] R. de Sousa Abreu, L. O. Penalva, E. M. Marcotte, and C. Vogel, Mol. BioSyst. **5**, 1512 (2009).
[74] M. E. Vogel C H, Nat. Rev. Gen. **13**, 227 (2012).
[75] N. Mehta and H.-Y. M. Cheng, J. Mol. Biol. **425**, 3609 (2013).
[76] E. Levine and T. Hwa, Curr. Opin. Biotechnol. **11**, 574 (2008).
[77] S. Brown, E. Kowalska, and R. Dallmann, Dev. Cell **22**, 477 (2012).
[78] J.-C. Leloup and A. Goldbeter, J. Biol. Rhy. **13**, 70 (1998).
[79] J.-C. Leloup and A. Goldbeter, Proc. Natl. Acad. Sci. USA **100**, 7051 (2003).
[80] D. B. Forger and C. S. Peskin, Proc. Natl. Acad. Sci. USA **100**, 14806 (2003).
[81] M. A. Lema, D. A. Golombek, and J. Echave, J. Theor. Biol. **204**, 565 (2000).
[82] S. Risau-Gusman and P. M. Gleiser, J. Theor. Biol. **307**, 53 (2012).
[83] B. Goodwin, Adv. Enzyme Regul. **3**, 425 (1965).
[84] J. Griffith, J. Theor. Biol. **20**, 202 (1968).